

INVESTIGATION OF THE BINDING AFFINITY OF RNA MOLECULES FOR
HYDROTALCITE AND MONTMORILLONITE AS POTENTIAL RNA
INTERFERENCE-BASED THERAPY DELIVERY SYSTEMS

by

Blanca V. Rodriguez, B.S.

A thesis submitted to the Graduate Council of
Texas State University in partial fulfillment
of the requirements for the Degree of
Master of Science
with a Major in Biochemistry
August 2015

Committee Members:

L. Kevin Lewis, Chair

Gary Beall

Karen Lewis

COPYRIGHT

by

Blanca V. Rodriguez

2015

FAIR USE AND AUTHOR'S PERMISSION STATEMENT

Fair Use

This work is protected by the Copyright Laws of the United States (Public Law 94-553, section 107). Consistent with fair use as defined in the Copyright Laws, brief quotations from this material are allowed with proper acknowledgment. Use of this material for financial gain without the author's express written permission is not allowed.

Duplication Permission

As the copyright holder of this work I, Blanca V. Rodriguez, authorize duplication of this work, in whole or in part, for educational or scholarly purposes only.

ACKNOWLEDGEMENTS

First and foremost, I'd like to thank my advisor and mentor, Dr. Kevin Lewis. It was truly a wonderful experience working with you this past year-and-a-half and I owe much of my growth as a scientist to you. I would also like to thank Dr. Corina Maeder for not only serving as a co-advisor to this project, but for continuing to be involved in my life as a friend and mentor. The immense support and encouragement that you have provided me for these past years have given me the confidence to pursue a career in research, and for that I will always be thankful. Dr. Gary Beall was also crucial in bringing this project to fruition and I would like to thank him for the guidance and extensive knowledge that he provided us with. I would also like to thank Dr. Karen Lewis for serving on my committee and for taking the time to work with me.

I am also extremely thankful to my lab mates and friends at Texas State who have supported me through this. I am so fortunate to have met such amazing friends during my time here.

I would also like to thank my family, who has supported me unconditionally throughout my journey at Texas State. Their continuous love and support has always motivated me to push myself and to reach my goals. None of this would have been possible without them and for that I am eternally grateful.

TABLE OF CONTENTS

	Page
ACKNOWLEDGEMENTS	iv
LIST OF FIGURES	vi
CHAPTER	
I. INTRODUCTION	1
II. MATERIALS AND METHODS	19
III. RESULTS AND DISCUSSION.....	27
IV. SUMMARY AND CONCLUSIONS.....	66
REFERENCES	69

LIST OF FIGURES

Figure	Page
1. Scale schematic of common nanoparticles and how they compare to cell components in size (2).....	2
2. Diagram of montmorillonite consisting of an octahedral sheet sandwiched between two tetrahedral sheets, responsible for MMT's 2:1 nature (13).....	4
3. This model shows the structural characteristics of montmorillonite (15)	5
4. Modes of binding between DNA and montmorillonite (17)	7
5. Schematic representation of the general structure of hydrotalcite (33).....	10
6. Schematic representation of the mechanism of intercalation of oligonucleotides with hydrotalcite (29).....	11
7. Proposed mechanism of cellular uptake for hydrotalcite (29).....	13
8. Schematic showing the difference between siRNA and miRNA pathways (42)	16
9. The incorporation of nanoparticle based delivery systems with RNA interference (46).....	17
10. Absorbance scans of hydrotalcite.....	31
11. Sequences and structures of the different types of nucleic acids used in this study....	33
12. RNA-HT centrifugation assays	35
13. Sedimentation and mobility shift assays were performed to quantitate the binding affinity of ssDNA 25mers, ssRNA 25mers, dsDNA 25mers and dsRNA 25mers for HT.....	37
14. Agarose gel (3%, 0.5X TB buffer) with RNAStr8 and RNALoop 54mers.	39
15. HT binding studies with RNALoop and RNAStr8 using centrifugation and electrophoretic mobility shift assays.....	41
16. Examples of structures and sequences of <i>E. coli</i> , <i>S. cerevisiae</i> , and human tRNAs (52).....	43

17. HT binding studies with tRNA using (A) centrifugation and (B) electrophoretic mobility shift assays.....	44
18. Schematic from Nakayama <i>et al.</i> showing the binding mode of DNA to HT from data collected by X-ray diffraction (34).	44
19. This schematic from Ishihara <i>et al.</i> shows that when HT is exposed to atmospheric air, the CO ₂ can interact with the interlayer water and exchange the ¹³ CO ₃ ²⁻ for ¹² CO ₃ ²⁻ (54).	45
20. Centrifugation assays performed with ssRNA (A ₂₆₀ ~1.0), 1 mg/mL HT, and the addition of sodium carbonate (Na ₂ CO ₃) or sodium sulfate (Na ₂ SO ₄) at 0, 1, 10, 100, or 500 mM concentration.....	46
21. RNA-MMT centrifugation assays	49
22. Na-MMT centrifugation assays with ssDNA, ssRNA, dsRNA, and dsRNA 25mers.....	51
23. Proposed cation bridging model by Franchi <i>et al.</i> illustrates the role of divalent cations during binding of MMT with single-stranded oligonucleotides and double-stranded oligonucleotides at pH >5 (55).....	52
24. Representation of the binding modes between RNA and magnesium as depicted by Misra and Draper (60).....	54
25. This figure from Essington M. E. shows an example of outer-sphere complexation between the montmorillonite siloxane surface and a hydrated cation (58).....	55
26. Adsorption assays using RNAstr8 and RNALoop to Na-MMT.....	56
27. Proposed modes of interaction between nucleic acids and montmorillonite include intercalation between sheet platelets, binding to the surface or edges of MMT, or tactoid exfoliation upon adsorption.....	58
28. tRNA adsorption assays using Na-MMT with and without the addition of NaCl or MgCl ₂	59
29. Adsorption assays involving 25mers and Ca-MMT.....	60
30. tRNA adsorption to Ca-MMT was assayed.....	62

31. Electrophoretic mobility shift assays performed on ssRNA 25mers with increasing HT concentrations.....	63
32. Conceptual schematic from Saeki <i>et al.</i> illustrating the possible ways Tris interacts with DNA molecules and montmorillonite (63)	64

CHAPTER I

INTRODUCTION

With the advent of nanotechnology in the past 15 years, many distinct scientific fields such as agriculture, electronics, biomaterials and medicine have benefitted immensely from their integration with this novel area of research. The focus on nanotechnology research has led to the advancement of knowledge about the chemical, physical, and biological properties of nanoparticles. Nanoparticles differ from bulk materials in that they are defined as being ≤ 100 nm in at least one dimension (1-4). This feature is precisely what makes them so attractive for use in a wide range of applications. Such a minute size causes nanoparticles to have a high surface-area-to-mass ratio, thereby increasing their chemical reactivity. Nanoparticles have an increased ability to interact with biological systems due to their similarity in size to biological components (Figure 1). An efficient uptake of molecules through the cell membrane requires their size to be at or below 200 nm, thus penetrations of nanoparticles is enabled by their size (1). Additionally, nanoparticles have been shown to partake in lysosomal escape after endocytosis (1). It is then without surprise that nanoparticles have become interesting candidates as delivery tools for drugs or biomolecules.

Medicinal nanotechnology aims to advance the field of drug/biomolecule delivery by improving targeting and biocompatibility while minimizing the toxicity of the carrier. Particularly for targeted therapy, nanoparticle carriers offer the ability to bind, protect, and deliver molecules to their destined site. Nanoparticles can achieve controlled release of the drugs/biomolecules through changes in the physiological environment by triggers such as changes in pH levels, temperature, or via enzymatic activity (2).

Nanoparticles vary in size and in chemical composition and because of the large amount of nanoparticles that exist, it is of great interest to find and optimize nanoparticles that are suitable for therapeutic purposes. Optimal carriers would not only be able to deliver and release the drug/biomolecule into targeted cells, but should also be biodegradable and have an appropriate lifespan to maximize their therapeutic activity. The eventual fate of the nanoparticles is of great importance as accumulation of foreign particles can be detrimental to cells. Moreover, nanoparticles intended for biomedical applications must be nontoxic and must not elicit an immune response. Nanoclays in particular stand out as potential candidates to fulfill those parameters.

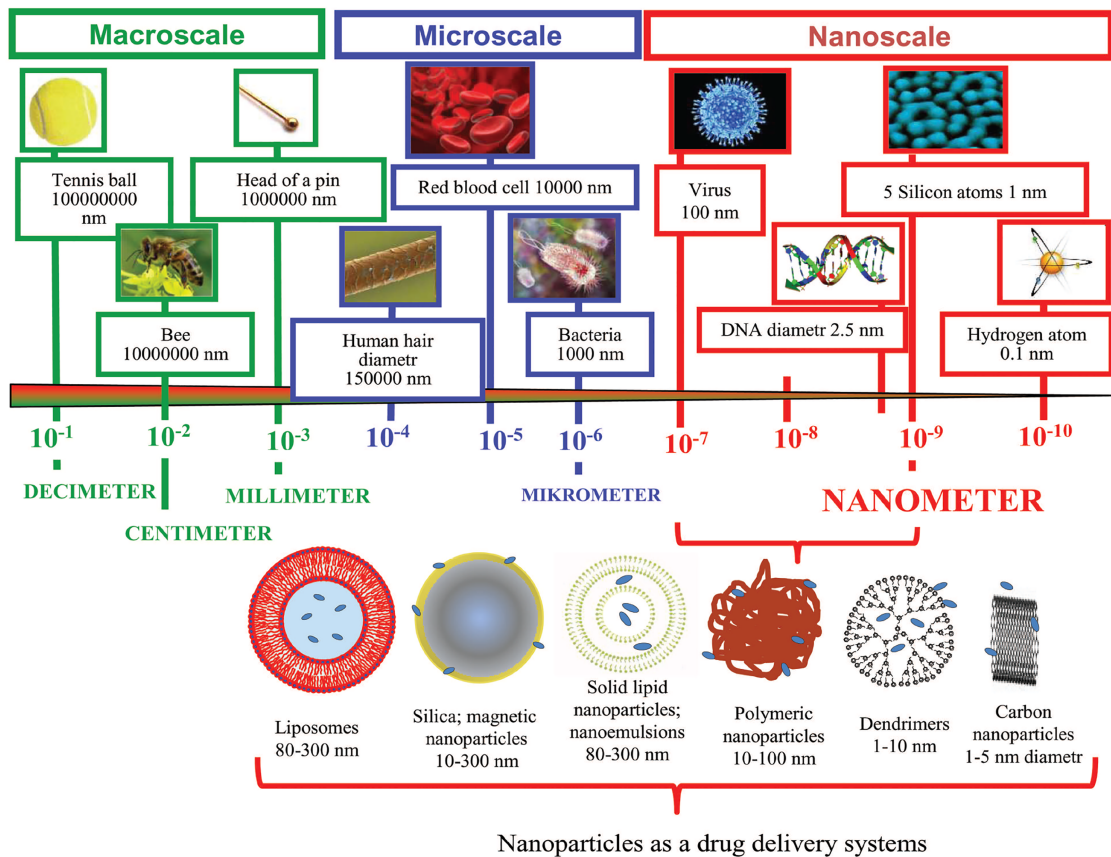


Figure 1. Scale schematic of common nanoparticles and how they compare to cell components in size (2).

Nanoclays are inorganic layered silicates, usually aluminosilicates. They can either be natural clay minerals found abundantly in nature or clays that can be easily synthesized in the lab. As such, they are quite inexpensive and have been shown to be very useful in a multitude of applications. Studies on these types of nanoclays have been extensively carried out for biomedical purposes (5-9). The incessant interest in nanoclays for medicinal purposes arises from their exceptional properties such as their low toxicity, high ability to adsorb biomolecules, high surface area, and their high ion exchange capacity. This high ion exchange capacity allows them to be easily modified, thereby altering their surface properties for distinct uses. Small ionic molecules can be exchanged easily on both the surface and the interlayer space of the clay sheets. The capacity of nanoclays to perform this exchange is completely dependent on the type of nanoclay used.

Two commonly studied nanoclays, hydrotalcite (HT) and montmorillonite (MMT), have high anion (100-500 mEq/100g) or cation (80-150 mEq/100 g) exchange capacities, respectively (7-10). This allows them to adsorb to large amounts of biomolecules. MMT is classified as a cationic nanoclay due to its high exchange capacity of cations, while HT is an anionic clay capable of exchanging anions. Traditionally, modified montmorillonite has been used for a variety of applications spanning dermatology, cosmetic products, and acting as anti-inflammatory agents; it has been used for food packaging materials and as excipients for pharmaceutical agents. Recently, both of these nanoclays have shown great promise for the delivery of biomolecules and drugs into mammalian cells (4-9).

Montmorillonite is a 2:1 layered aluminosilicate consisting of the general formula $M_x(Al_{2-y}Mg_y)Si_4O_{10}(OH)_2 \cdot nH_2O$ (11). It exists as a sheet-like structure and is approximately 1 nm thick and can be up to 1000 nm wide, with a surface area of approximately 700 m²/g (12). MMT is classified as a 2:1 layered mineral based upon the number of tetrahedral and octahedral sheets it contains, as well as their structural arrangement (Figure 2).

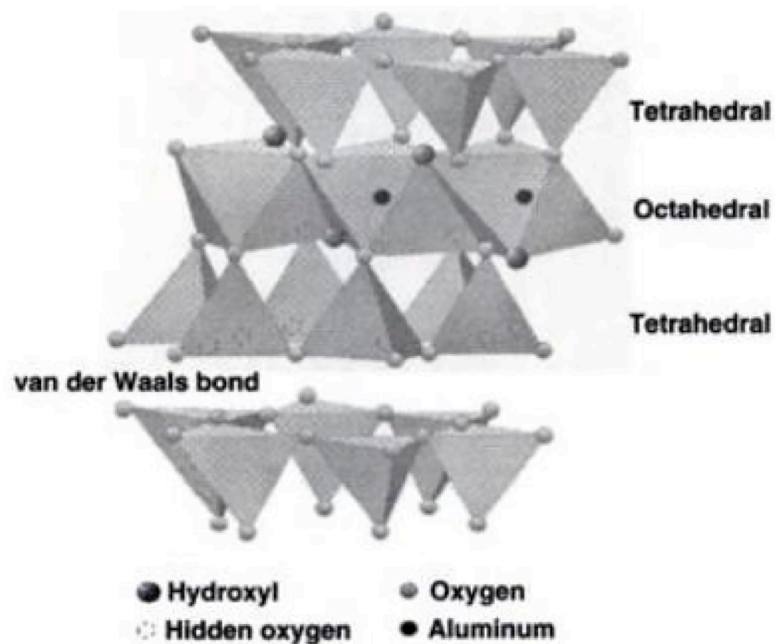


Figure 2. Diagram of montmorillonite consisting of an octahedral sheet sandwiched between two tetrahedral sheets, responsible for MMT's 2:1 nature (13).

Montmorillonite is composed of two outer silica tetrahedral sheets layered between a central alumina octahedral sheet to form a sandwich-like structure (Figure 3). The octahedral layer contains aluminum and magnesium atoms, which coordinate to oxygen atoms and hydroxyl groups. The silica atoms coordinate to oxygen atoms. Isomorphous substitutions (replacement of one structural cation for another of comparable size) occur in the octahedral layer by the substitution of the trivalent

aluminum ions by divalent cations, such as Mg^{2+} . The tetrahedral layer also undergoes isomorphous substitutions of the Si^{4+} by Al^{3+} , although with less frequency (11, 14). These substitutions induce a net negative charge on the clay. Exchangeable positive counterions such as alkaline earth metals can then adsorb in the interlayer spaces of montmorillonite between the 2:1 layers among water molecules to balance the negative charge.

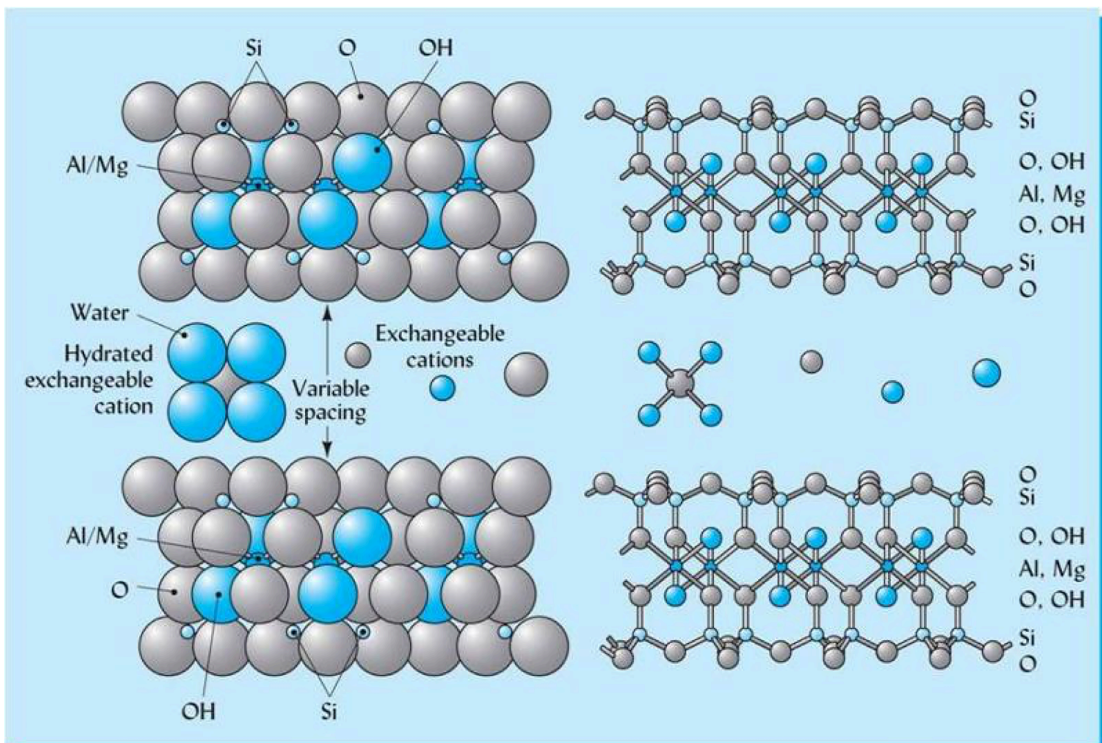


Figure 3. This model shows the structural characteristics of montmorillonite (15).

Montmorillonite is a smectite clay, meaning that the material swells and expands upon hydration causing stacking, or tactoid formation, to occur. Montmorillonite tactoids are not uniform in size, shape, or charge. The characteristics of montmorillonite tactoids vary based on the type of cation exchanged and the pH of the environment (11). The interlayer spacing of MMT, also known as the gallery, ranges in size based on the level of

hydration. For example, water saturation causes the gallery to expand up to 2 nm, while an anhydrous environment will reduce the gallery to less than 1 nm (13). The interlayer space of MMT is important as cations that adsorb can interact with negatively charged particles, such as drugs or biomolecules. The intercalation of biomolecules into nanoclays is an important feature as this strategy can help to protect the drug/biomolecule from chemical and enzymatic degradation. For example, nucleases could degrade DNA/RNA before they can transfer genetic information or be incorporated into gene regulation pathways for therapy.

One of the most common strategies of delivering DNA into cells is through the use of viral vectors such as retroviruses, adenoviruses, and adeno-associated viruses. While successful in many gene delivery applications, a very important caveat for using viruses is that they can eventually integrate into the genome, become reactive, and provoke mutagenesis and carcinogenesis. For this reason, the current knowledge gaps for inert non-viral delivery vehicles such as nanoclays need to be closed as nanoclays could prove to be much better delivery vehicles than viral vectors.

Many studies have been performed to evaluate the ability of anionic biomolecules such as DNA to adsorb to homoionic montmorillonite. Hou *et al.* presented evidence that DNA adsorption on MMT occurs through electrostatic interactions, ligand exchange (wherein the hydroxyl groups of the ribose and the phosphate groups at the end of a DNA molecule adsorb to the clay) (16), and cation bridging (Figure 4) of the DNA phosphate backbone and exchangeable cations (17). Beall *et al.*, found that homoionic montmorillonite can intercalate single-stranded DNA between its sheets through cation bridging (7). Furthermore, they showed that adding divalent cations, such as magnesium,

to solution can enhance the adsorption of DNA to MMT. They also found that despite DNA adsorbing to both sodium montmorillonite (Na-MMT) and calcium montmorillonite (Ca-MMT), DNA bound more readily to Ca-MMT than to Na-MMT. Modulating the kind of exchangeable cations in MMT has proven to have significant effects on its ability to bind to biomolecules.

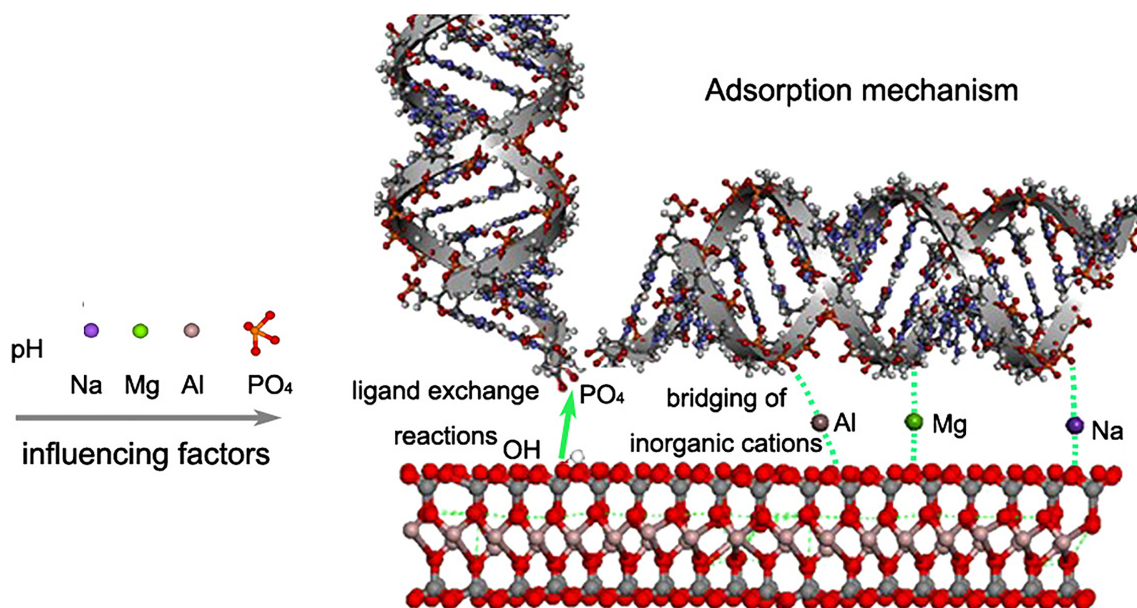


Figure 4. Modes of binding between DNA and montmorillonite (17).

Various researchers have assessed montmorillonite for its potential as a drug/biomolecule delivery vehicle. Lin *et al.* demonstrated the ability of modified montmorillonite to protect DNA from nuclease degradation by monitoring the expression of enhanced green fluorescent protein in human dermal fibroblast cells (18). The DNA delivered into the cells contained the reporter gene and was successfully expressed after being carried by a modified form of MMT (18). Kawase *et al.* performed a series of experiments to evaluate the effectiveness of Na-MMT as a gene delivery system for plasmid DNA encoding EGFP (19). Their initial *in vitro* studies using intestinal epithelial

cells (IEC-6) resulted in expression of EGFP on cells transfected by the Na-MMT/DNA preparations (19). They also prepared clay/plasmid DNA complexes and administered them orally to mice. EGFP production was detected in the mice that received the MMT/DNA preparations only, no EGFP was detected in mice that received a naked plasmid preparation. This supports the observation that montmorillonite is able to protect DNA from nucleases and from pH changes in the intestine (19). In 2010, Kevadiya *et al.* compared the controlled release of vitamin B1 and vitamin B6 in *in vitro* assays after being intercalated into MMT (20). The composite was gelled into alginate nanocomposite beads, released in phosphate buffer solution of pH 7.4, and measurements of the concentration of the released vitamin B1 and vitamin B6 revealed a pH-dependent controlled release from the vitamin B1/B6-MMT alginate beads. Lin *et al.* reported successful intercalation of a chemotherapy drug, 5-fluorouracil (5-FU), into MMT layers by optimizing time, pH, temperature and concentration (18). Many other examples of successful intercalation of drugs such as ibuprofen (21), promethazine chloride (22), timolol maleate (23) and paclitaxel (24), and their controlled delivery by montmorillonite can be found in the literature.

Montmorillonite has garnered positive attention as a potential gene carrier system due to its low toxicity. Recently, Maisanaba *et al.* evaluated the cytotoxicity effects of Na-MMT and an organically modified MMT on Caco-2, human intestinal cells (25). Their *in vitro* studies showed no toxic effects for the Na-MMT exposed cells, while significant morphological effects on the Golgi apparatus and nucleolar segregation were observed with the modified-MMT treated cells (25). The lack of cytotoxicity from Na-MMT agreed with previous *in vivo* and *in vitro* studies that have demonstrated no

significant toxicity of homoionic montmorillonite on animal and human subjects (26-28). In fact, the Federal Drug Administration has classified clay (bentonite containing montmorillonite) as generally recognized as safe (GRAS) (<http://www.accessdata.fda.gov/scripts/fdcc/?set=SCOGS>). Nonetheless, the Maisanaba *et al.* study highlights the importance of assessing the toxicity profile for every modified nanoclay used in medicinal or food packaging applications as different modifiers can induce different levels of toxicity (25). Particularly for cancer therapy, developing suitable nanocarriers is an undertaking that has shown much promise.

Hydrotalcite is an anionic nanoclay that is a member of the layered double hydroxide family (LDH) and has been found to be promising for gene delivery and controlled drug/DNA release systems (5, 29-32). Similar to MMT, HT is commonly used in a variety of different applications, such as water treatment, flame-retardants, sorbents, cosmetics, and as enteric delivery vehicles for antacids (7, 31). HT can be described with the formula $[M^{II}_{1-x}M^{III}_x(OH)_2]^{x+}(A^{m-})_{x/m} \cdot nH_2O$ ($x = 0.2-0.4$; $n = 0.5-1$), where M^{II} can be divalent metal cations such as Mg, Ni, Co, M^{III} represents trivalent metal cations such as Al and Fe, and A^{m-} are exchangeable anions such as CO_3^{2-} , SO_4^{2-} and Cl^- . HT is structurally similar to a brucite layer, $Mg(OH)_2$, as each Mg^{2+} ion is octahedrally surrounded by six OH^- ions and every octahedral subunit pair share edges, leading the two-dimensional layer to expand infinitely (29-32). Isomorphic substitution of Mg^{2+} ions by Al^{3+} ions gives these layers a net positive charge. This charge is balanced by water and by the anions that are accommodated in the interlayer gallery via electrostatic bonding such as hydrogen bonding (29-32). Figure 5 shows how a three-dimensional structure of hydrotalcite is formed by the stacking of the brucite-like layers.

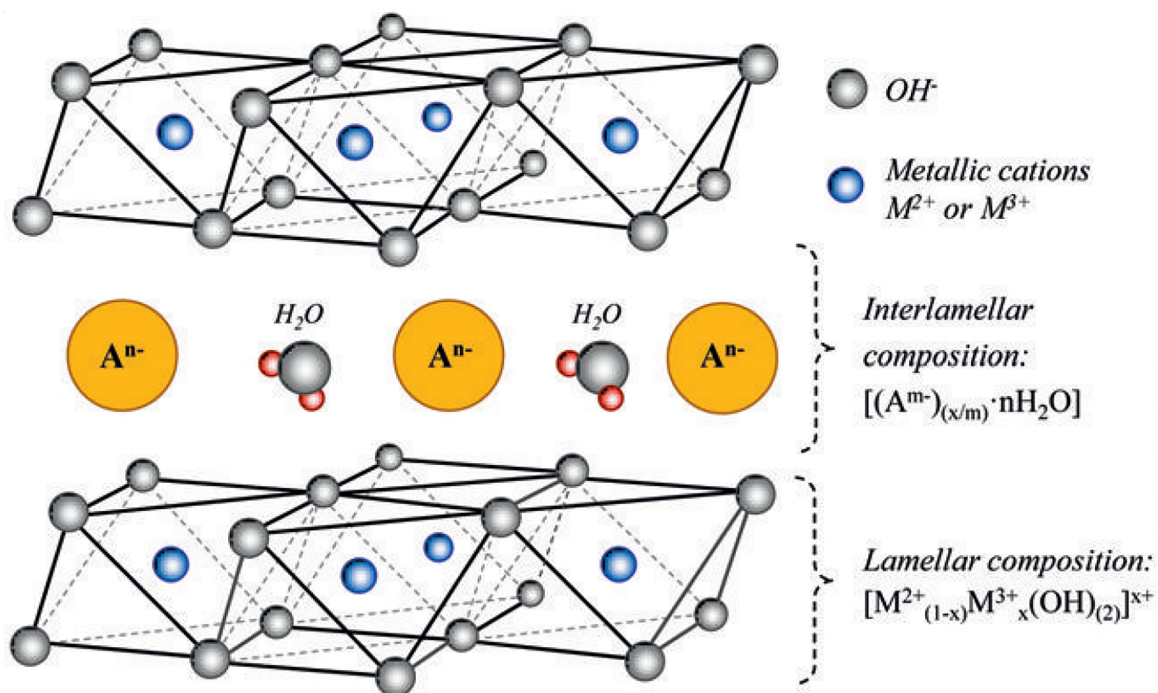


Figure 5. Schematic representation of the general structure of hydrotalcite (33).

HT is a strong candidate for a biodelivery system by nearly every metric: low cost, good biocompatibility, chemical versatility, anionic exchange capacity, low toxicity to mammalian cells, easy synthesis, high drug loading density and transportation, cellular uptake, and the ability to provide full protection for biomolecules and drugs. Extensive studies have shown that hydrotalcite can intercalate with different types of anions, such as inorganic anions, complex anions, anionic polymers, drugs, and organic biochemical anions such as amino acids and nucleic acids (29, 31). These interactions occur by an anion exchange mechanism in which the anions residing in the interlayer space are replaced by the aforementioned anions (Figure 6) (34). This intercalation allows for the protection from degradation of drugs/biomolecules (34).

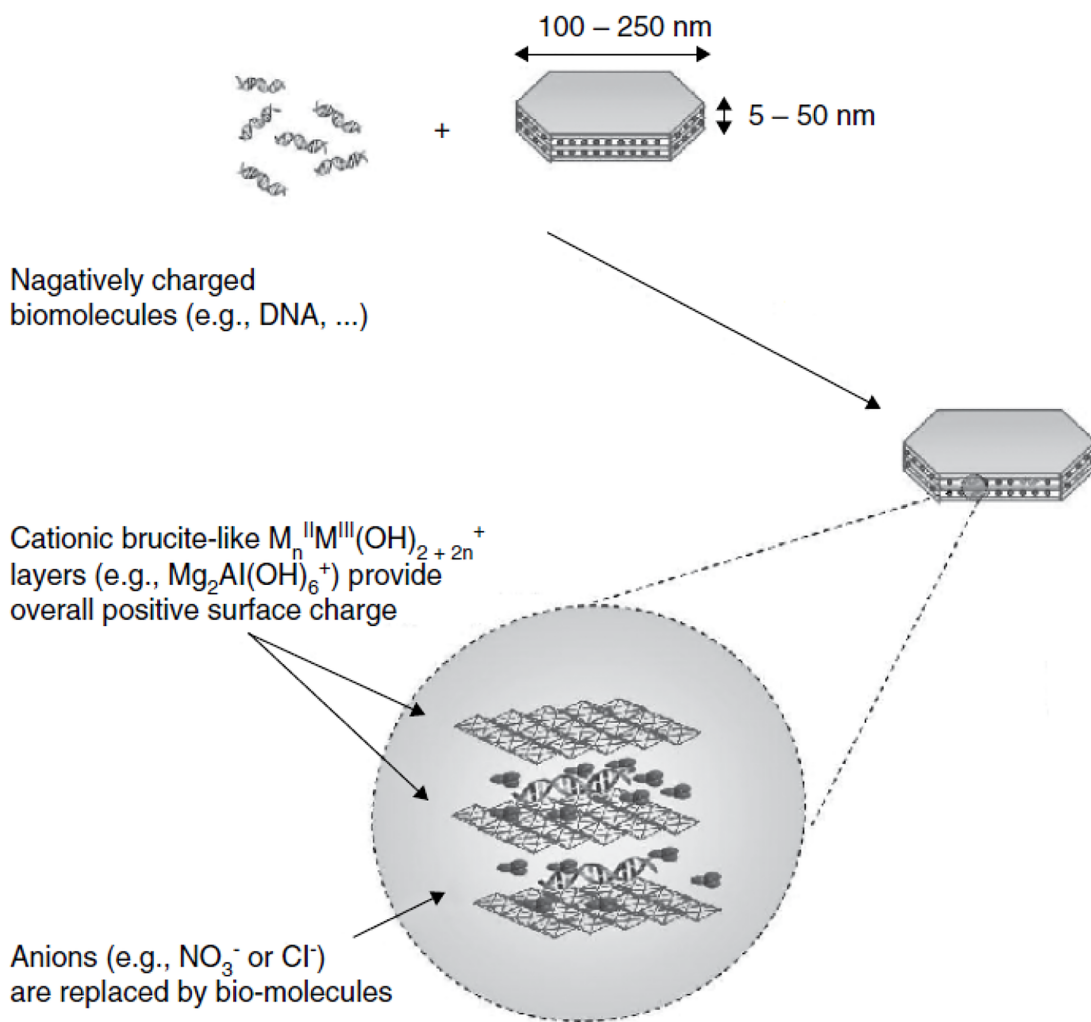


Figure 6. Schematic representation of the mechanism of intercalation of oligonucleotides with hydrotalcite (29).

A critical aspect of gene delivery by nanoparticles is their ability to penetrate the cell membrane. Efficient uptake of oligonucleotides through the cell membrane can be mediated by intercalation of the oligomer into hydrotalcite (29). Although the mechanism by which HT crosses the cell membrane has not been fully elucidated, evidence has shown that HT can internalize via a common energy-dependent endocytosis pathway known as clathrin-mediated endocytosis (5). Figure 7 shows the potential pathway of hydrotalcite once it crosses the cell membrane. It gets enveloped into endosomes at

different stages of transport and subsequently is deposited into lysosomes for degradation. The schematic depicts hydrotalcite as releasing the oligonucleotide in the nucleus on the basis of the numerous studies that have shown effective gene expression from transfected DNA/HT complexes (29). The overall positive charge of HT/ DNA hybrids is an immense advantage for using HT as a delivery vehicle due to the HT/DNA complex adhering the negatively charged cell membrane. No additional modifications or functional groups are required for the HT to efficiently enter the cell. While clathrin-mediated endocytosis is the mechanism by which HT is believed to transfect DNA into cells by, the mechanism of DNA unloading into the nucleus remains unclear. One possibility set forward by Sokolova *et al.* involves the possibility that the nanoparticles are dissolved by acid in the endosomal vesicles (1).

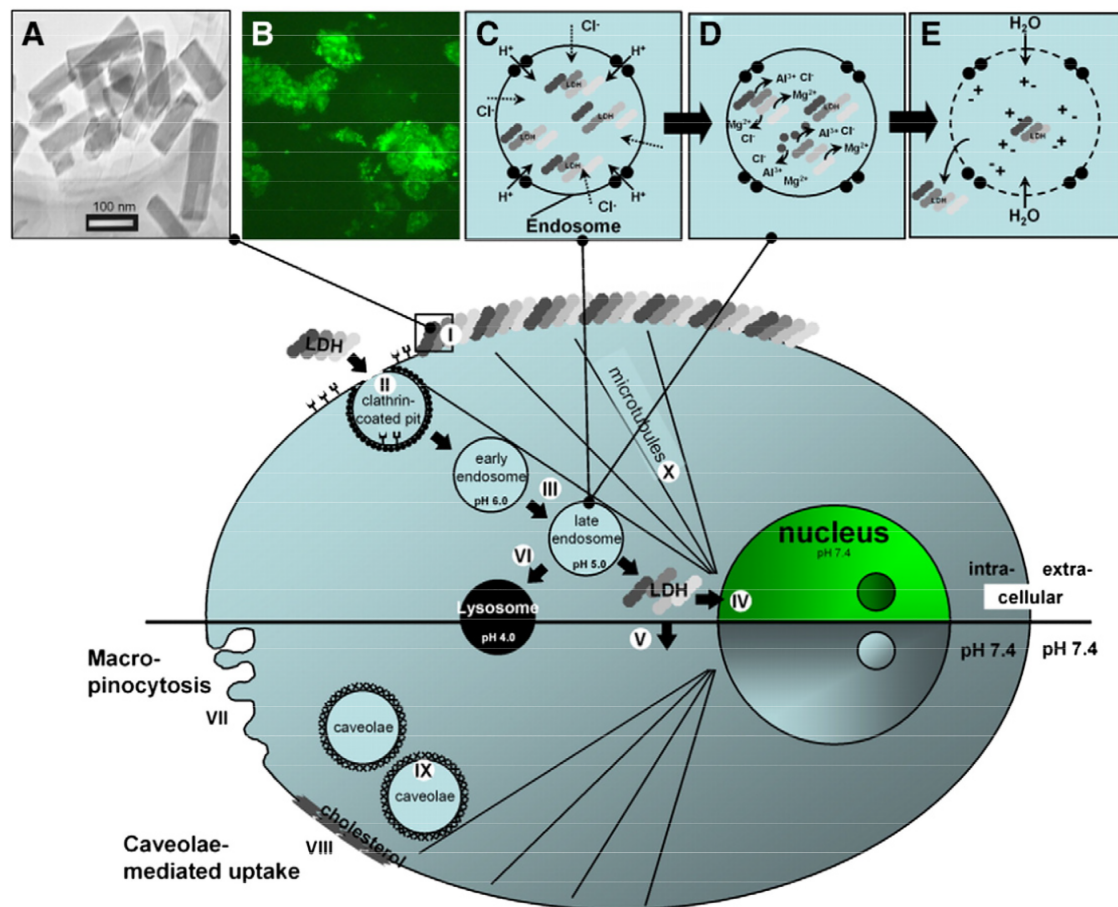


Figure 7. Proposed mechanism of cellular uptake for hydrotalcite (29).

The success in using HT as a delivery vehicle for biomolecules and drugs has been well documented by many researchers. Kim *et al.* recently showed that the intercalation of both methotrexate and 5-FU into the hydrotalcite framework increases the effectiveness in suppressing tumors (35). The Barahuie *et al.* group successfully delivered two anti-cancer drugs, chlorogenic acid and protocatechuic acid, using modified hydrotalcite (36). Also, Ma *et al.* loaded the prodrug disuccinatocisplatin into the hydrotalcite interlayer by ion-exchange (37.). The adsorption capability of hydrotalcite to single-stranded and double-stranded DNA was evidenced by a study performed by Sanderson *et al.* in 2013 (8). They noted that adsorption was dependent on the conditions

of synthesis of the hydrotalcite as well as on the charge density of both the DNA molecules and the hydrotalcite (8). Li *et al.* successfully transfected DNA plasmids encoding the enhanced green fluorescent protein into NSC 34 (mouse motor neuron cells) (38). Indeed, hydrotalcite has been shown to be an efficient delivery vehicle for drugs and DNA.

Although a few examples of RNA molecules being delivered into cells after intercalation by HT exist, low delivery efficiency has been observed during the studies (39-41). Interestingly, Li *et al.* (2014) demonstrated that the combination of siRNA and anticancer drugs such as 5-FU, loaded onto hydrotalcite enhances the delivery efficiency into cancerous cells (41) further demonstrating the advantage of combining drugs with biomolecules for cancer therapy using nanoclays.

While the adsorption capability and binding mode of DNA molecules to HT have been widely studied using adsorption assays and structural techniques such as X-ray diffraction and SEM analysis, past work on the binding of HT to RNA is very limited. It has been proposed by Ladewig *et al.* that an increasing size of DNA leads to lower loading efficiency onto the hydrotalcite, probably due to the DNA molecule forming a tertiary structure and supercoiling (31). This structural change results in the inability of DNA to intercalate in HT, thereby reducing the adsorption of the biomolecule to the nanoclay. Therefore, it would be necessary to analyze the adsorption and binding affinity of different RNA molecules to hydrotalcite as RNA interference therapy gains traction. In contrast, even small RNA molecules can form secondary and tertiary structures. A direct comparison of the difference of small DNA molecules versus small RNA molecules, with and without secondary structure, could reveal important factors in determining adequate

nanoparticle delivery vehicles for emerging RNA interference therapies.

RNA interference is a silencing mechanism that occurs in eukaryotic cells as a gene regulation event (42-45). This process is intricately linked to the gene silencing that derives from microRNAs (miRNAs). miRNAs are encoded in the nucleus of cells as long double-stranded hairpin RNA molecules that are subsequently cleaved by an enzyme (Drosha) into pre-miRNA. The pre-miRNA molecule is then exported out of the nucleus to the cytoplasm by association with the enzyme exportin 5. Pre-miRNA is processed once again by another enzyme, Dicer, creating a miRNA duplex. The miRNA associates with a complex of proteins that contain catalytic activity, termed the RISC complex. The final processing events occur during the miRNA's association with RISC, where the antisense strand of the miRNA is cleaved from the sense strand and remains bound to the RISC complex. The anti-sense strand acts as a guide to then target the complementary mRNA strand, blocking gene expression of the specific mRNA (Figure 8).

Although similar, RNAi differs in key aspects from miRNA silencing. RNAi is not an endogenous mechanism and requires the transfection of a synthetic double-stranded RNA, a small interfering RNA (siRNA), or a DNA plasmid encoding siRNA into cells by viral or non-viral vectors. Another distinction between the two is that the primary gene silencing mechanism of siRNAs is cleavage of mRNA while miRNAs can also inhibit mRNA translation by binding to and blocking translation (Figure 8). Both siRNAs and miRNAs are approximately 21-24 nucleotides in length after processing by Dicer.

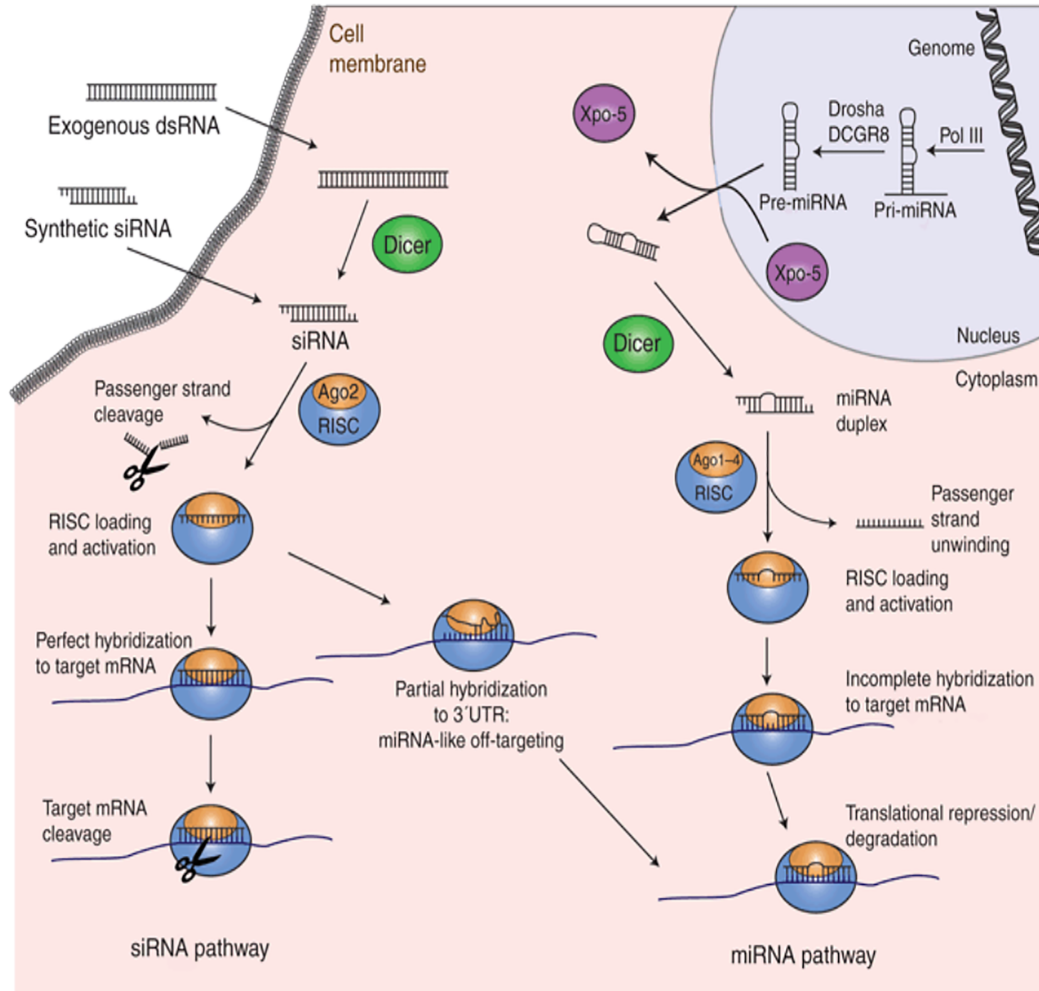


Figure 8. Schematic showing the difference between siRNA and miRNA pathways (42).

RNAi is a technique commonly used to knock down levels of a specific protein during expression-based studies using either synthetic siRNA or miRNA. However, in recent years RNAi-based therapy has generated much interest. *In vitro* and *in vivo* studies have shown that RNAi therapy can be used to target single-gene diseases as well as diseases that are caused by the overexpression of specific proteins (42-45). Similar to gene therapy applications, RNAi-based therapy would benefit immensely from optimized and biocompatible nanoparticles that can efficiently deliver small synthetic non-coding RNAs into cells. Although it is important for the nanoclays to efficiently deliver genes to

the nucleus for gene therapy, RNAi strategies have more leeway as it is sufficient to deliver siRNA into the cytoplasm where it can be incorporated into the RNAi pathway (42-45). Strides have been made in the pursuit of finding optimal nanoparticles for RNAi (Figure 9). However, the common viral and non-viral vectors have shown drawbacks, which is where the study of nanoclays could be beneficial as a delivery vector for RNAi-based therapies.

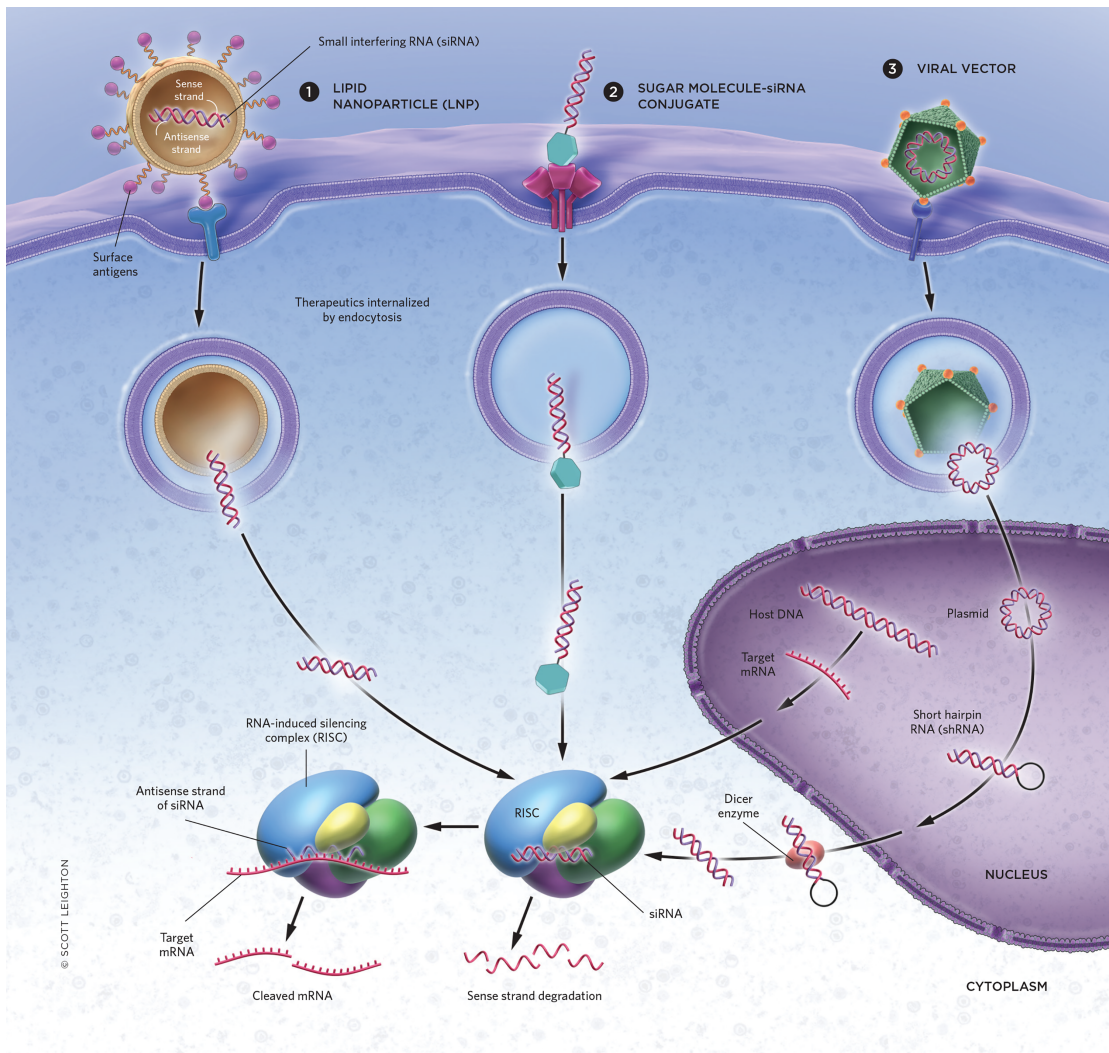


Figure 9. The incorporation of nanoparticle based delivery systems with RNA interference (46).

The aim of this project was to analyze the associations of RNA molecules with hydrotalcite and montmorillonite. Different types of RNA molecules with secondary and tertiary structure were evaluated for their binding affinity and adsorption to HT and MMT. The purpose of this study was to bring insight into the binding preference of HT and MMT for different RNA molecules. This work could help accelerate the development and optimization of RNA delivery systems for RNAi-based therapy.

CHAPTER II

MATERIALS AND METHODS

Materials

Hydrotalcite ($[\text{Mg}^{2+}_{.82}\text{Al}^{3+}_{.18}(\text{OH})_2]\text{Cl}^{-.18}$) with a charge density of 300 meq/100 g was prepared through precipitation followed by hydrothermal heating in a Parr reactor at 150°C. Powdered homoionic sodium montmorillonite (Na-MMT) was obtained from Southern Clay Products, Inc. (Gonzalez, TX). The following DNA and RNA oligonucleotides were purchased from Integrated DNA Technologies (Coralville, IA): ssDNA 25mer Pvu4a (AAATGAGTCACCCAGATCTAAATAA), its complement cPvu4a (TTATTTAGATCTGGGTGACTCATTT), ssRNA 25mer PvuRNA (AAATGAGTCACCCAGATCTAAATAA), its complement cPvuRNA (TTATTTAGATCTGGGTGACTCATTT), dsRNA 54mer RNALoop (AAAUGAGUCACCCAGAUCUAAAUAAGUAAUUAUUUUAGAUCUGGGUGACUCAUU), and ssRNA 54mer RNAStr8 (AAAUGAGUCACCCAGAUCUAAAUAAGUAAAAAUGAGUCACCCAGAUCUAAAUAA). Transfer RNA (tRNA) from *Escherichia coli*, Tris base, tricine, triethanolamine, magnesium chloride, sodium chloride, sodium carbonate, and sodium sulfate were purchased from Sigma Aldrich (St. Louis, MO). Low MW DNA Ladder and dsRNA ladder were purchased from New England Biolabs (Ipswich, MA). Agarose was obtained from Gold Biotechnology (St. Louis, MO). Boric acid was purchased from JT Baker (Center Valley, PA). SYBR Gold was purchased from Invitrogen Life Sciences (Grand Island, NY). Eppendorf Flex-Tubes (1.5 mL) were purchased from Eppendorf (Hauppauge, NY). All electrophoresis experiments were performed using 11 cm x 14 cm

Horizon gel rigs (Labrepco) and an Amersham/GE Healthcare EPS 601 power supply (Horsham, PA).

Hydrotalcite light spectroscopy analysis

Spectroscopic absorbance measurements and scans of HT were performed using a Cary 100 Bio UV-Vis spectrophotometer. A 1.5 mL quartz cuvette was used for UV spectra measurements. A 50 $\mu\text{g/mL}$ HT sample mixed with water was scanned using a wavelength range of 200 nm – 800 nm. A time-dependent spectroscopy scan was also performed on the 50 $\mu\text{g/mL}$ HT sample at 200 – 300 nm. The time points measured were the following: 0, 1, 5, 10, 20, and 30 min. Five HT samples (50 $\mu\text{g/mL}$, 25 $\mu\text{g/mL}$, 12.5 $\mu\text{g/mL}$, 6.25 $\mu\text{g/mL}$, and 3.125 $\mu\text{g/mL}$) were scanned from 200 – 300 nm and their absorbance measurements at 260 nm were plotted into a best-fit trendline using Microsoft Excel in order to generate a standard curve and equation. Four HT concentrations (2 mg/mL, 1 mg/mL, 0.5 mg/mL and 0.25 mg/mL) were centrifuged at 21,000 x g for 5 min, 1 mL of supernatant was removed and the A_{260} was measured. The concentration of HT after centrifugation was calculated by using Beer-Lambert's Law on the standard curve equation.

Double-stranded DNA/RNA preparation

To make double-stranded DNA (dsDNA) used for HT assays, 525 ng Pvu4a was mixed with 525 ng cPvu4a plus ddH₂O and 5 mM Tris (pH 7.4) in a total volume of 1 mL for a total of 1,050 ng dsDNA. To make double-stranded DNA (dsDNA) for MMT assays, 1,050 ng Pvu4a was mixed with 1,050 ng cPvu4a plus ddH₂O and 5 mM Tris (pH

7.4) in a total volume of 1 mL for a total of 2,100 ng dsDNA. For double-stranded RNA (dsRNA), 600 ng PvuRNA, 600 ng cPvuRNA, ddH₂O and 5 mM Tris (pH 7.4) were mixed in a total volume of 1 mL for a total 1,200 ng dsRNA. The solutions were placed in a heating block for 5 min at 100 °C and were then allowed to anneal at RT for 30 min. RNALoop was prepared by mixing 3.1 µg/µL RNALoop with 5 mM Tris (pH 7.4) and water up to 500 µL. The sample was heated for 4 min at 90°C and allowed to cool at room temperature for 30 min. Confirmation of successful dsRNA, dsDNA, and RNALoop formation was analyzed using agarose gel electrophoresis with 3.5% agarose and 0.5X Tris/borate (45 mM/45 mM) running buffer. Gels were run for approximately 10 min at 350V as described by Sanderson *et al.* (47). The gel was stained using 0.5 µg/mL ethidium bromide. A low MW DNA ladder was run with the dsDNA and RNALoop samples while a dsRNA ladder was used for the analysis of dsRNA samples.

Preparation of DNA/hydrotalcite and RNA/hydrotalcite solutions for adsorption assays

HT-ssDNA solutions were prepared by mixing 75 µL of HT (0.25, 0.05, 1, 2, or 4 mg/mL), 3 µL Pvu4a DNA (750 ng/µL, for a final $A_{260} = 0.5$) and ddH₂O in a final volume of 150 µL. For dsDNA binding studies, 52.5 µL dsDNA was added to the dsDNA/HT solutions.

HT-ssRNA solutions were prepared by mixing 75 µL of HT (0.25, 0.05, 1, 2, or 4 mg/mL), 10 µL PvuRNA (300 ng/µL, for an $A_{260} = 0.5$) and ddH₂O in a final volume of 150 µL. For dsRNA, 30 µL dsRNA was added. HT-54mer RNA mixtures were prepared by adding 19 µL RNAStr8 (300 ng/µL, final $A_{260} = 1$) and 14.5 µL RNALoop (300

ng/ μ L, for a final $A_{260} = 1$). For tRNA-HT assays, 10 μ L tRNA (300 ng/ μ L) was added. Assay mixtures were shaken for 5 min and centrifuged at 21,000 x g for 5 min at RT.

DNA/HT and RNA/HT adsorption analysis

Immediately after centrifugation, the top 60 μ L of the supernatant of each sample was transferred into a new Eppendorf tube. The absorbance of the unbound DNA/RNA was measured using UV light spectroscopy at 260 nm. The average of each DNA-HT and RNA-HT series was calculated. The % nucleic acid bound to the HT was calculated by subtracting the average absorbance of unbound nucleic acid from the original nucleic acid-only absorbance. The difference was then divided by the original nucleic acid-only absorbance. Microsoft Excel software was used to analyze the adsorption results.

Preparation of RNA/hydrotalcite for mobility shift assays

For ssRNA-HT electrophoretic mobility shift assays (EMSAs), 300 ng ssRNA was mixed with ddH₂O, and HT (0, 0.02, 0.04, 0.08, 0.16, 0.32, or 0.64 mg/mL) in a final volume of 20 μ L. Four μ L of 30% glycerol was added later before loading the gel. dsRNA EMSAs contained 300 ng nucleic acid and HT concentrations of 0, 0.16, 0.32, 0.64, 1.28, 2.56, and 5.12 mg/mL in a final volume of 24 μ L. RNALoop EMSAs contained 100 ng nucleic acid, while RNAStr8 assays contained 150 ng and both were mixed in HT concentrations of 0, 0.04, 0.08, 0.16, 0.32, and 0.64 mg/mL in a final volume of 20 μ L. tRNA EMSAs consisted of 150 ng tRNA and HT concentrations of 0, 0.16, 0.32, 0.64, 1.28, and 2.56 mg/mL. After letting the mixtures sit for 5 min at RT, 18 μ L of each sample was loaded into the gel.

Agarose gel electrophoresis

The EMSA gels were designed to effectively separate small oligonucleotides using agarose gels with the parameters described by Sanderson *et al.* (47). ssRNA (25mer), dsRNA (25mer), RNALoop (54mer), and RNAStr8 (54mer) EMSAs were performed using 3.5% agarose gels while tRNA was run on a 1.2% gel. Agarose gels were made in 45-50 mL 0.5X TB buffer. All samples were run at 350V, except tRNA, which was run at 400V. All RNA samples were run for 4-10 min. SYBR Gold (10,000X) was diluted to 4X in 40 mL ddH₂O and was layered on top of the gels to completely cover them in stain. All gels were stained in SYBR gold for 15 min and were destained in water with shaking for 20 min. EMSA gels were imaged using the ProteinSimple Red Imaging System. Band densitometry analysis for each gel was performed using ImageJ software (<http://imagej.nih.gov/ij/>). The dissociation constant (K_D) was calculated by transferring the data generated from ImageJ to Microsoft Excel and creating a best fit trendline equation. The trendline equation, $y = mx + b$, was rearranged into $K_D = (0.5 - b)/m$, where $y = K_D$ and $x = 0.5$ to quantitate the dissociation constant.

HT salt competition assays and displacement

The salts that were used for these sets of experiments were sodium carbonate and sodium sulfate. For the competition assays, 5 μ L ssRNA (300 ng/ μ L) was mixed with ddH₂O, 50 μ L HT (2 mg/mL), and 0 mM, 1 mM, 10 mM, 100 mM, or 500 mM concentrations of each salt in a total volume of 100 μ L. The displacement assays were prepared using the same amounts of ssRNA, ddH₂O, HT, and salt concentrations. However, the RNA, water, and HT were mixed first and the salts were added last in the

latter assays. The samples were vortexed for 5 min and centrifuged for 5 min at 21,000 x g. The A_{260} of each sample was measured using a spectrophotometer, and the percentage of RNA bound was calculated using the previously described method.

Preparation of nucleic acids + Na-MMT/Ca-MMT solutions for adsorption assays

Calcium montmorillonite (Ca-MMT) was prepared by mixing equal volumes of 1 M CaCl_2 with Na-MMT and centrifuging at 34,000 x g for 30 minutes at 4°C. The resulting pellet was subsequently washed with cold water three times and was resuspended in water to match the initial volume. Confirmation of successful cation-exchange was performed by measuring the A_{230} of Na-MMT before the addition of CaCl_2 , and a final A_{230} measurement was taken after the resuspension step. ~90% MMT was consistently recovered. Na-MMT and Ca-MMT were sonicated using a Sonics & Materials, Inc Vibracell VC130 Sonicator. The clay was sonicated at an amplitude of 40 for 4 min.

Each MMT centrifugation assay required a set of control tubes. Control tubes contained 75 μL Na-MMT or Ca-MMT + 75 μL ddH₂O. Salt experiment control tubes consisted of 75 μL Na-MMT/Ca-MMT + 0.1, 1, 10, or 100 mM NaCl/MgCl₂ and up to 150 μL ddH₂O final volume.

MMT-ssDNA solutions were prepared by mixing 75 μL of Na-MMT or Ca-MMT (0.2, 0.5, 1.25, or 3.125 mg/mL), 7 μL Pvu4a DNA (750 ng/ μL , for final $A_{260} = 1$) and ddH₂O in a final volume of 150 μL . For dsDNA binding studies, 52.5 μL dsDNA was added to the dsDNA/MMT solutions. MMT-ssRNA solutions were prepared by mixing 75 μL of Na-MMT or Ca-MMT (0.2, 0.5, 1.25, or 3.125 mg/mL), 20 μL PvuRNA (300

ng/ μ L, for final $A_{260} = 1$) and ddH₂O in a final volume of 150 μ L. For dsRNA, 60 μ L dsRNA was added. MMT-54mer RNA mixtures were prepared by adding 19 μ L RNAstr8 (300 ng/ μ L, for final $A_{260} = 1$) and 14.5 μ L RNAloop (300 ng/ μ L, for $A_{260} = 1$). For tRNA-MMT assays, 10 μ L tRNA (300 ng/ μ L, for $A_{260} = 1$) was added. Assay mixtures were shaken for 5 min and centrifuged at 25,000 x g for 1 hr at 4 °C using the Allegra 64R centrifuge. Salt studies were prepared with the same amount of Na-MMT/Ca-MMT and nucleic acids as above, with the addition of 0.1, 1, 10 and 100 mM NaCl or MgCl₂. Each assay consisted of 4 tubes to ensure results were replicable to calculate averages and standard deviations.

DNA/MMT and RNA/MMT adsorption analysis

Immediately after centrifugation, the top 60 μ L of the supernatant of each sample was transferred into a new Eppendorf tube. The absorbance of the unbound DNA/RNA was measured using UV light spectroscopy at 260 nm. The A_{260} of the control tubes was subtracted from the A_{260} of the experimental tubes in order to correct for absorbance contributions from the clay. The bound and unbound nucleic acid percentage was calculated as described in the HT adsorption analysis section.

MMT EMSAs

The Ca-MMT + ssRNA (200 ng) EMSA pilot assay was performed with 0.04, 1, 2.5, and 5 mg/mL Ca-MMT concentrations. The conditions were identical to those used for the HT EMSAs. An EMSA was also performed using 1X Tricine/Triethylamine (30

mM/30 mM) as the running buffer using a 3.5 % agarose gel. The gel was run at 150V for 5 min, and was stained for 20 min in SYBR Gold.

CHAPTER III

RESULTS AND DISCUSSION

The overarching goal of this study was to analyze the association of RNA molecules with the nanoclays hydrocalcite (HT) and montmorillonite (MMT). Specifically, we were interested in assessing the binding affinity of HT and MMT for different forms of RNA: single-stranded RNA (ssRNA) 25mer, double-stranded RNA (dsRNA) 25mer, dsRNA 54mer with a 4 nt loop (RNALoop), ssRNA 54mer (RNAstr8), and tRNA (a more complex dsRNA with three stem-loop regions). This research has determined the binding affinities of MMT and HT for RNA molecules and the data will contribute to the field of nanotechnology in the context of gene therapy, particularly for RNAi therapy.

UV spectroscopy is a valuable tool for quantitating different types of biochemical molecules in solution. A molecule's absorbance at a particular wavelength depends on its chemical properties. A linear relationship exists between the absorbance of many molecules and their concentration, allowing the use of Beer-Lambert's Law to calculate accurate concentrations from spectroscopy absorbance measurements. It has been established that nucleic acids absorb UV light strongly at 260 nm, therefore their concentration in solution is typically calculated by measuring the UV absorbance at this wavelength (48). As such, one of the methods used in this study to quantitate the amount of nucleic acid that binds to HT and MMT was by measuring the A_{260} of DNA or RNA present in the supernatant after centrifugation of a nucleic acid/nanoparticle mixture. Therefore, it was imperative to ensure that the spectroscopic analysis of DNA/RNA was

accurate and not affected by potential A_{260} measurement contributions from either MMT or HT.

Previous work by Beall *et al.* showed that homoionic montmorillonite exhibits a UV absorbance peak at 230 nm due to the Fe^{3+} found in the lattice of the MMT sheets (7). MMT was also shown to have strong absorbance at 260 nm. Further, MMT was shown to sediment inefficiently, indicating that a substantial amount of MMT remained in solution after centrifugation, which was shown to contribute to an overestimation of free nucleic acid measured from A_{260} readings. As a result, Beall *et al.* implemented an additional control in their DNA/MMT studies to circumvent the interference of MMT with the DNA A_{260} measurements (7). The design of the centrifugation assays used in the current study was modeled on the Beall *et al.* findings. This led us to investigate whether HT absorbs UV light and more specifically, if a significant amount of absorbance is present at 260 nm.

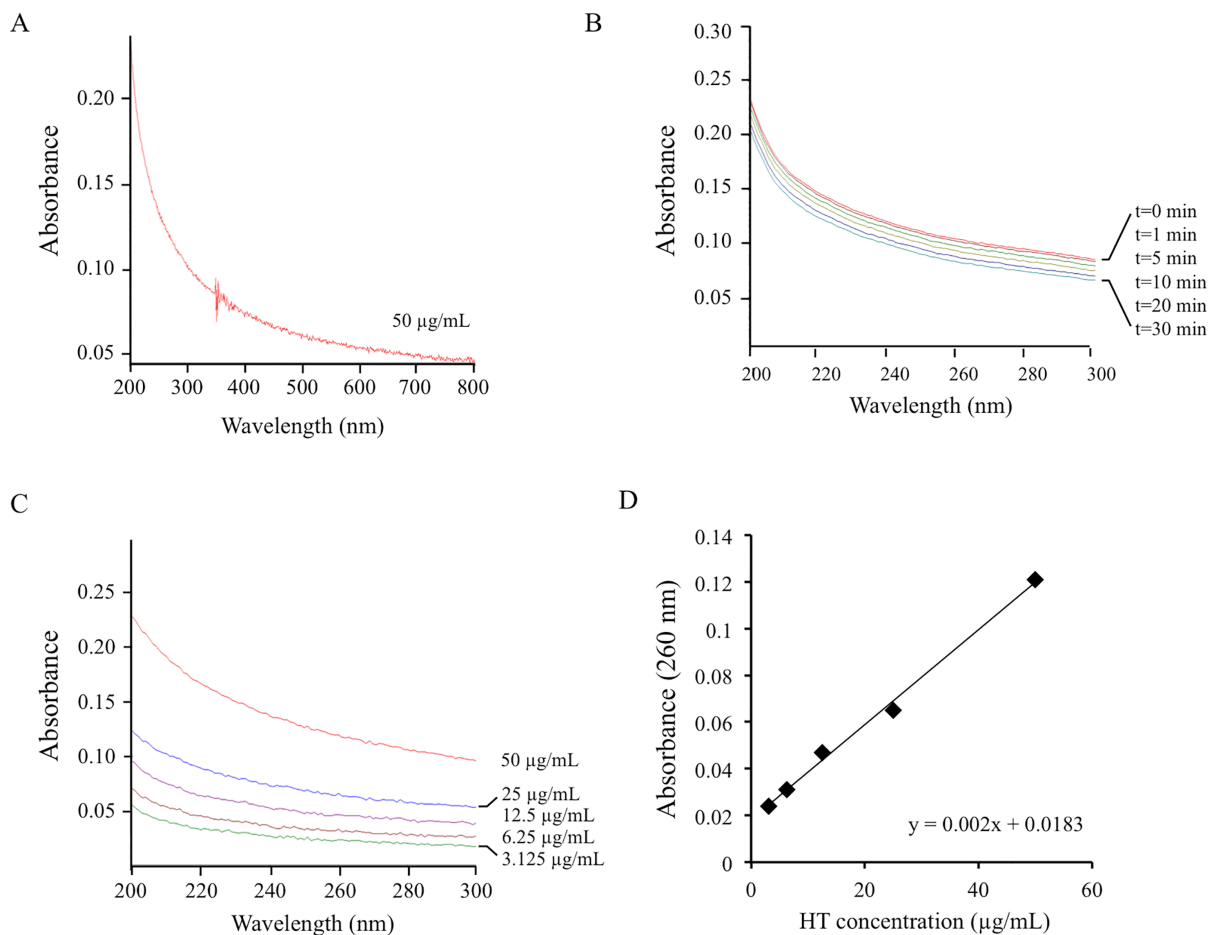
Unlike montmorillonite, hydrotalcite is not known to be a light absorbing species. Nonetheless, it was important to establish that hydrotalcite would not contribute to the A_{260} measurements, as was the case for MMT. To characterize the absorbance spectra for hydrotalcite at a low concentration, a 50 $\mu\text{g/mL}$ HT sample was subjected to an absorbance scan from 200 – 800 nm. Figure 10A shows the absorbance scan, which revealed an HT absorbance over most of this range and an inverse relationship between increasing wavelengths and absorbance. Because the HT nanoparticles may be capable of scattering light, some of the apparent absorbance may also be due to this phenomenon.

Centrifugation binding assays typically involve the use of multiple samples whose absorbance is measured shortly after centrifugation. As a result, even though the

measurements can be made quickly, not all samples are tested at the same time. HT particles naturally sediment toward the bottom of tubes when suspended in aqueous solutions, which may increase the variability of measurements. We assessed whether taking absorbance readings at different time points would have a significant effect on the absorbance of the sample, considering the disparity in the amount of time it takes to obtain spectroscopic measurements of samples. As per Figure 10B, only slight changes were observed in absorbance of 50 $\mu\text{g}/\text{mL}$ HT between 0 and 30 min. This result indicates that sedimentation will not affect the absorbance of HT solutions if measurements are taken relatively quickly, e.g., within 5 minutes or less.

Dilutions of the 50 $\mu\text{g}/\text{mL}$ HT sample were prepared and their absorbances were measured from 200 – 300 nm (Figure 10C). From this data, the A_{260} for each concentration was found and plotted on a best-fit trendline (Figure 10D). The linear relationship between HT concentration and absorbance allowed us to generate a trendline equation according to Beer-Lambert's law (Absorbance = $\epsilon c L$, where ϵ is the extinction coefficient, L is the path length of the light, and c is the concentration of the solute). This relationship was used in a set of experiments to find out how easily HT particles can be sedimented using a standard biochemistry laboratory microcentrifuge. The experiments used similar HT concentrations to those that would be employed for the physical binding assays of nucleic acids to HT (0.25, 0.5, 1, and 2 mg/mL). These experiments characterized the ability of HT to sediment after a 5 min spin. The data is tabulated in Figure 10E and shows that at the highest HT concentration, 2 mg/mL, a 5 min spin at 21,000 x g is sufficient for 99.8% of HT to be removed from the supernatant. At 0.25 mg/mL and 0.5 mg/mL HT, 100% of the hydrotalcite was removed. These results

indicate that, while un sedimented hydrotalcite absorbs light between 200 – 300 nm, a 5-minute spin is sufficient for the HT to sediment exceptionally well and as a result, any absorbance at 260 nm becomes insignificant and would not contribute substantially to the nucleic acid absorbance measurements.



E

Starting [HT]	After Centrifugation		
	A_{260}	[HT]	HT Removed
2 mg/mL	0.025	3.35 µg/mL	99.8%
1 mg/mL	0.044	12.9 µg/mL	98.7%
0.5 mg/mL	0.011	0 µg/mL	100%
0.25 mg/mL	0.015	0 µg/mL	100%

Fig 10. Absorbance scans of hydrotalcite. (A) A 50 µg/mL HT solution was scanned from 200 nm – 800 nm. (B) A 50 µg/mL HT solution was scanned from 200 – 300 nm at different times (0, 1, 5, 10, 20, and 30 min) after an initial vortexing step. (C) Absorbance scans for 50, 25, 12.5, 5.25, and 3.125 µg/mL HT solutions were performed from 200 nm – 300 nm; (D) The A_{260} data was plotted on a best-fit trendline to create a standard curve. (E) Determination of the efficiency of sedimentation of HT particles after centrifugation for 5 min at 21,000 x g.

Figure 11 shows the sequence information and structure of the nucleic acids used in this study. Although the main focus of the study was to assess the binding of RNAs to HT and MMT, we included single-stranded DNA and double-stranded DNA in order to have a direct comparison in binding affinity to a nucleic acid that has been established to have high affinity for nanoclays. We used short ssRNAs, dsRNAs, and RNAs with stem-loops that mimic either siRNAs or miRNAs, which are RNA molecules involved in regulation of protein synthesis by RNA interference. In addition, we also included tRNA, which folds into an L-shaped tertiary structure, in order to investigate the importance of RNA structure to the binding affinity with HT and MMT.

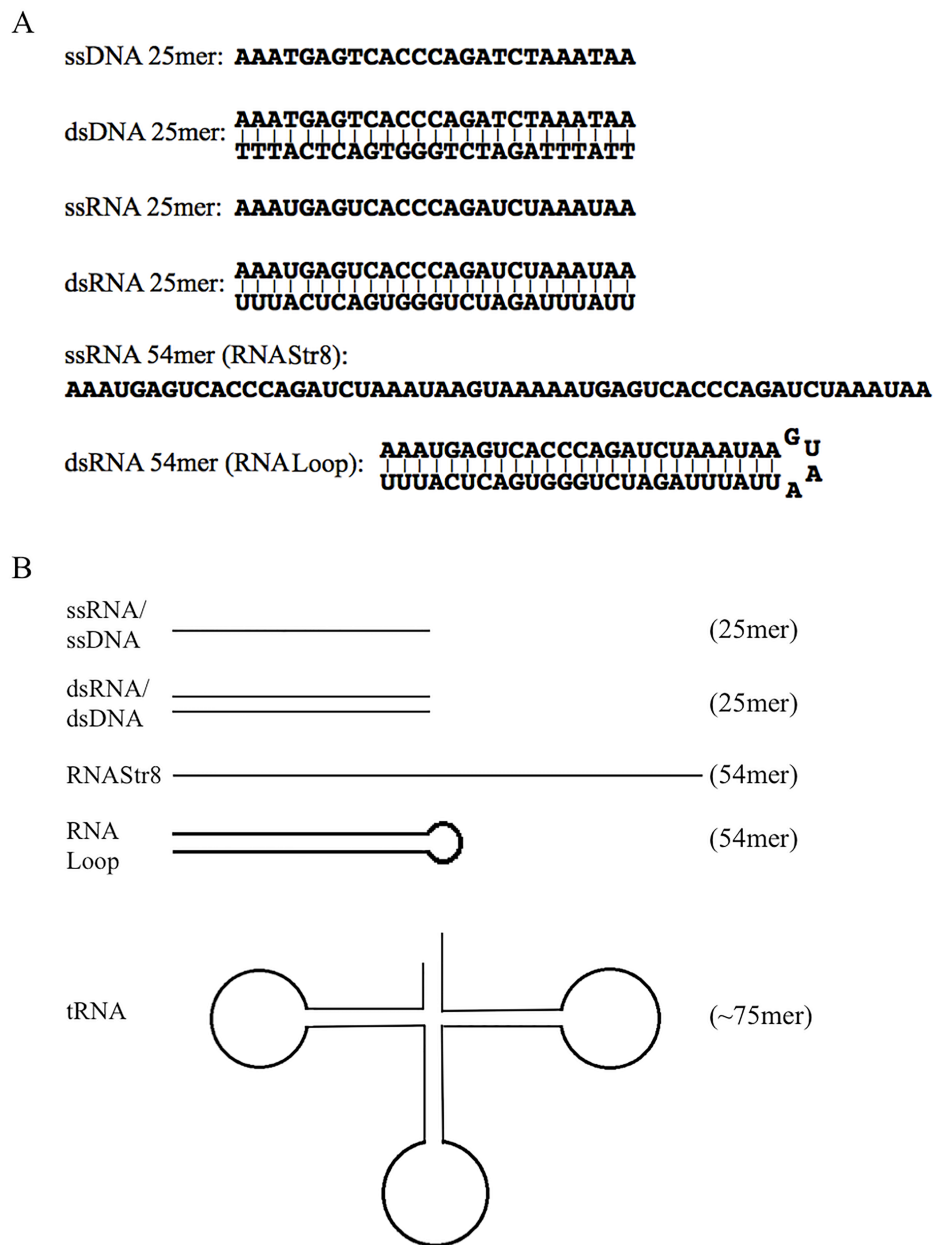


Fig 11. Sequences (A) and structures (B) of the different types of nucleic acids used in this study.

As RNAi therapy gains traction as a potential genetic therapeutic tool, the search for suitable RNA carriers increases. HT has been proposed in studies and reviews as a strong candidate for delivery of drugs and biomolecules (5, 6, 8, 29-32, 38). The interactions between DNA and HT have been the focus of previous extensive studies (8),

but there is limited literature on the binding of nanoclays to RNA in the context of gene delivery. Assessing whether RNA binds to HT is a basic and fundamental step in using HT as an RNA carrier for RNAi therapy applications.

In order to investigate the adsorption of nucleic acids to HT we employed centrifugation assays. By mixing the nucleic acids with HT in water and spinning the samples for 5 min at 21,000 x g, we were able to quantitate the separation of the free nucleic acids from the nucleic acids that adsorbed to HT by measuring the A_{260} of the supernatant after the spin (Figure 12). The centrifugation assays showed that no significant difference exists between the binding of ssDNA and ssRNA to HT (Figure 13A; averages and standard deviation from 4 assays for each concentration of HT are plotted). Also, binding curves for dsDNA and dsRNA were similar. At 1 mg/mL and 2 mg/mL HT, ssDNA and ssRNA each exhibited ~90% adsorption. HT at 1 mg/mL appeared to be a saturation point for the binding of ss nucleic acids to HT as the binding was not improved after a 2-fold increase in HT concentration (Figure 13A and 13B). In contrast to the ss nucleic acids, only 50% of the dsDNA and dsRNA was bound at 1 mg/mL HT. This represents a 2-fold adsorption decrease at 1.0 mg/mL HT compared to ss nucleic acids.

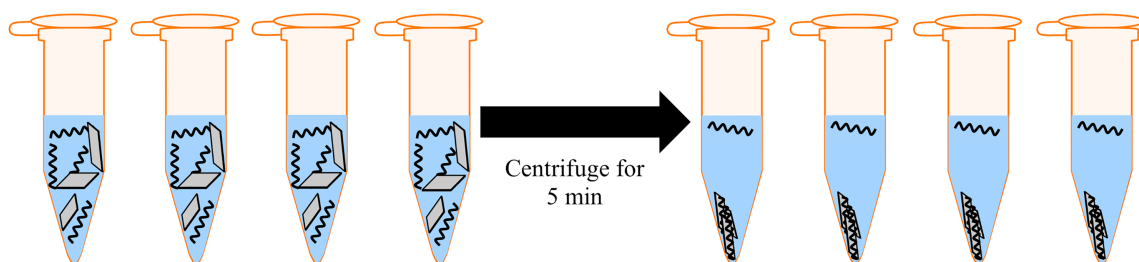


Fig 12. RNA-HT centrifugation assays. RNA ($A_{260} = 0.5$) was mixed with HT (0, 0.125, 0.25, 0.5, 1.0 or 2.0 mg/mL) and ddH₂O. Sedimented HT with bound RNA formed a pellet after a 5 min spin at 21,000 x g. Unbound RNA remained in solution.

To confirm the data from the sedimentation studies in Figure 13A and to determine a dissociation constant for the binding of HT to RNA, the binding affinity of HT for RNA was investigated through electrophoretic mobility shift assays (EMSA).

EMSAs are typically used to monitor the interaction between two moieties. Although polyacrylamide gels are commonly used to separate small oligonucleotides, we have employed agarose gels in an effective manner by following the parameters set forth by Sanderson *et al.* (8). For the HT EMSAs, 3.5% agarose gels were used in order to separate the small RNA oligonucleotides. The gels were run at 350V (400V for tRNA) for 4-10 minutes using 0.5X TB buffer and stained using SYBR Gold. The SYBR Gold stained the RNA but not the HT, which allowed visualization of the free RNA band as it migrated down the gel. As shown in Figure 13C, free RNA migrated to the bottom of the gel and exhibited a bright band. The bright band gradually disappeared as the concentration of HT increased. At 0.16 mg/mL HT, more than half of the ssRNA band disappeared, indicating its association with HT. For dsRNA, the band intensity reduction to less than half of the original intensity became apparent after 0.32 mg/mL HT. The factors that contribute to the disappearance of the free RNA band, the appearance of

smears above the free RNA band, as well as the formation of an RNA band in the well, involve the increased mass of the RNA and its charge neutralization. As RNA binds to the HT, which is a mixture of molecules of different sizes that have a sheet-like structure, the resulting complexes were not able to efficiently sieve through the agarose pores. Furthermore, the charge neutralization would also reduce the speed of migration towards the positive electrode.

In addition to supplying qualitative data, EMSAs can also provide quantitative results. We performed densitometry analysis on the bands of each EMSA agarose gel using Image J software, plotted the data in Microsoft Excel, and generated a best-fit trendline equation. The trendline equation was used to calculate the dissociation constant of the RNA-HT, which was defined as the concentration of HT at which the free RNA was reduced to 50% of initial levels, indicating that 50% of the RNA was bound to HT particles. This was accomplished by rearranging the $y = mx + b$ trendline equation into $K_D = (0.5 - b)/m$, where $y = K_D$ and $x = 0.5$. Three or four gels were run, apparent K_D values were calculated, and the results were averaged.

HT centrifugation studies showed a 2-fold increase in binding affinity between HT and ssRNA compared to the binding affinity of HT for dsRNA (Figure 13A and 13B). This 2-fold difference was further supported by the electrophoretic mobility shift assays (EMSAs), which showed HT-ssRNA with a K_D of 0.16 mg/mL and HT-dsRNA with a K_D of 0.39 mg/mL, roughly a 2-fold difference (Figure 13C and 13D). A low K_D indicates a strong affinity between two moieties; therefore ssRNA displayed approximately twice the affinity for HT as dsRNA.

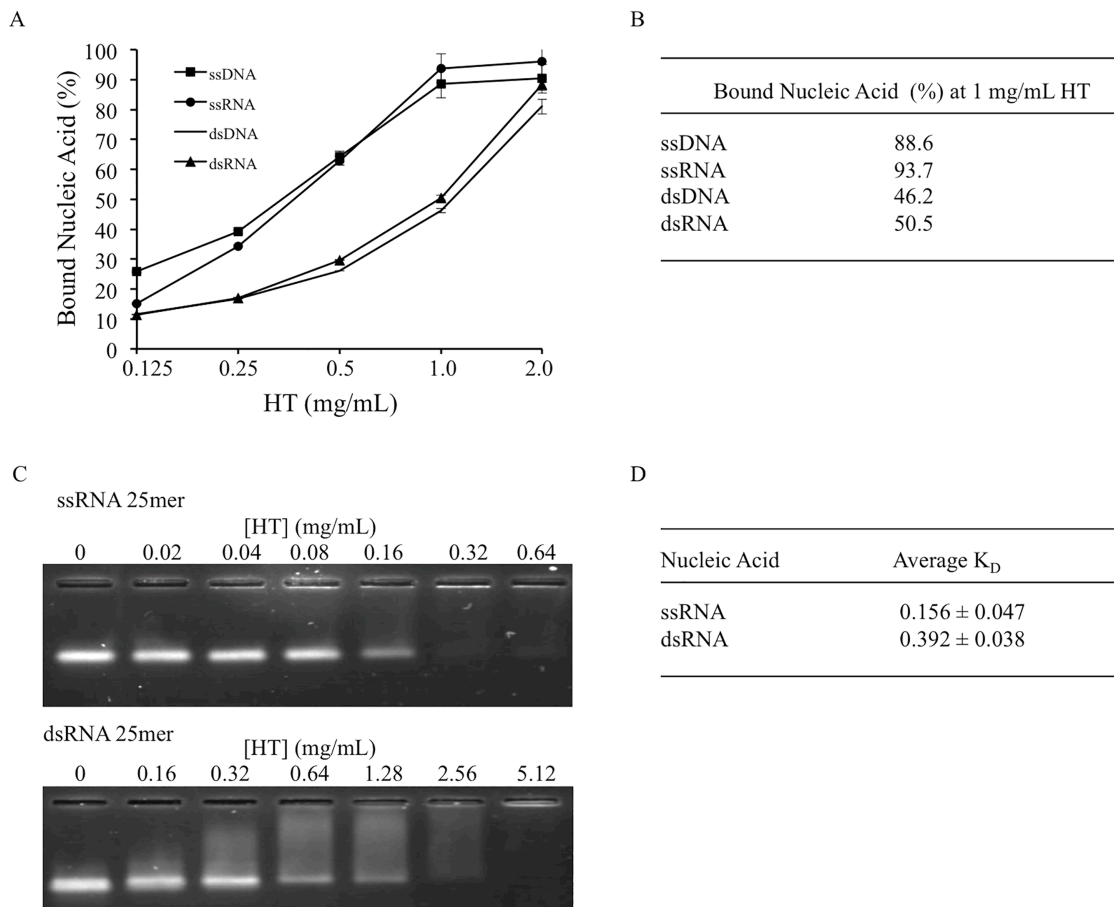


Fig 13. Sedimentation and mobility shift assays were performed to quantitate the binding affinity of ssDNA 25mers, ssRNA 25mers, dsDNA 25mers and dsRNA 25mers for HT. (A) Comparison of the % binding of nucleic acids to HT after mixing for 5 min and spinning for 5 min. (B) Data from centrifugation studies was tabulated to directly compare the binding of ss nucleic acids to ds nucleic acids with hydrotalcite at 1 mg/mL. (C) Representative electrophoretic mobility shift assays performed on ssRNA 25mers and dsRNA 25mers with increasing HT concentrations. Top gel: *Lane 1*, ssRNA (300 ng); *lanes 2-7*, ssRNA (300 ng) + 0.02, 0.04, 0.08, 0.16, 0.32, or 0.64 mg/mL HT, respectively. Bottom gel: *Lane 1*, dsRNA (300 ng); *lanes 2-7*, dsRNA (300 ng) + 0.16, 0.32, 0.64, 1.28, 2.56, or 5.12 mg/mL HT, respectively. (D) The apparent K_D values for ssDNA and dsRNA were determined by performing densitometry analysis on 3 or 4 EMSA gels using ImageJ software and generating a trendline equation in Microsoft Excel, and averaging the calculated K_D values. Averages and standard deviations are shown.

The results from the ssRNA and dsRNA assays suggested that there are determining factors that affect the binding affinity of RNA for HT since ssRNA had a 2-fold greater binding affinity to HT than dsRNA. One explanation could be that the increased number of overall negative charges on the dsRNA 25mer (-50) compared to the ssRNA 25mer (-25) affects its binding to HT. Another explanation could be that the dsRNA structure prevented the double helical dsRNA from binding as effectively to HT and perhaps from being incorporated as easily into the interlayer spaces.

With this in mind, we designed centrifugation and EMSA assays using two RNA molecules that would have the same overall negative charge but different structures. The RNALoop 54mer spontaneously folds upon itself to form 25 bp of double-stranded RNA with a 4 nt loop at one end, similar to miRNA (Figure 11B). The RNAStr8 54mer is single-stranded and has no regions of complementary bases within itself, which prevents the formation of secondary structures. To verify that RNALoop was fully annealed, a sample of the RNALoop RNA was analyzed on a 3% agarose gel and its migration was compared to a low molecular weight DNA ladder and to single-stranded RNAStr8 (Figure 13, lanes 1 and 2). Running RNALoop on an agarose gel revealed that the oligonucleotide was mostly double-stranded after simply resuspending it in ddH₂O. After a heating and cooling step (see Methods), almost all of the RNA became double-stranded (Figure 13, lane 4).

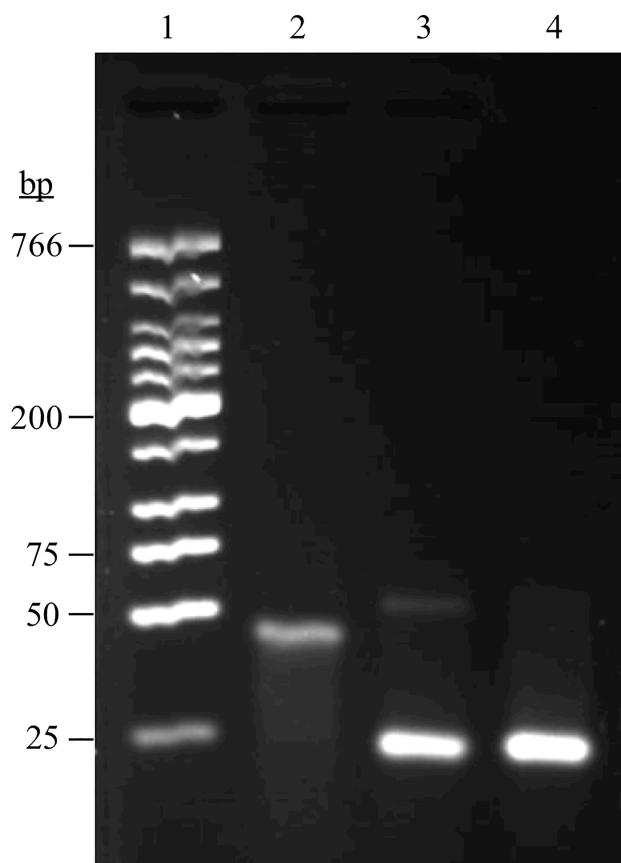


Figure 14. Agarose gel (3%, 0.5X TB buffer) with RNAStr8 and RNALoop 54mers. *Lane 1*, low molecular weight DNA ladder; *lane 2*, RNAStr8 (ssRNA 54mer); *lane 3*, RNALoop (dsRNA 54mer) in water; *lane 4*, RNALoop and 5 mM Tris (pH 7.4), heated at 90°C for 4 min, cooled for 30 min at RT.

The results from the centrifugation assays using the two 54mers indicated that RNALoop and RNAStr8 have similar adsorption to HT. For example, 70.7% of the RNALoop and 85.2% of the RNAStr8 was bound to HT at 1 mg/mL (Figure 15B and 15D). Interestingly, when the binding of RNAStr8 was compared directly to ssRNA, both RNA molecules appeared to have the same adsorption to HT (Figure 15A). Despite RNAStr8 having a potential -54 overall negative charge, its adsorption to HT was similar to that of the ssRNA 25mer that possesses a -25 overall negative charge. At the same time, binding of RNAStr8, a single-stranded 54mer, is similar to that of RNALoop, a

double-stranded RNA. These results suggest that total charge is not a major factor and that single-stranded vs. double stranded character is also not the main factor.

Furthermore, the data suggest that the total length is not critical, at least for small nucleic acids.

The EMSA data obtained by averaging results from 3 or 4 gels showed that RNA_{Loop} had a 0.131 K_D while RNA_{Str8} had a K_D of 0.194, with overlapping standard deviations (Figure 15C and 15E). In summary, the centrifugation experiments indicated an 18.6% difference (70.7 % vs 85.2%) at 1 mg/mL HT and the EMSAs pointed to only a 38.8% difference (0.131 vs. 0.194) between binding affinities of the single-stranded and double-stranded 54mers. These results suggest that the affinities of the single-stranded and double-stranded 54mers for HT do not differ strongly from one another.

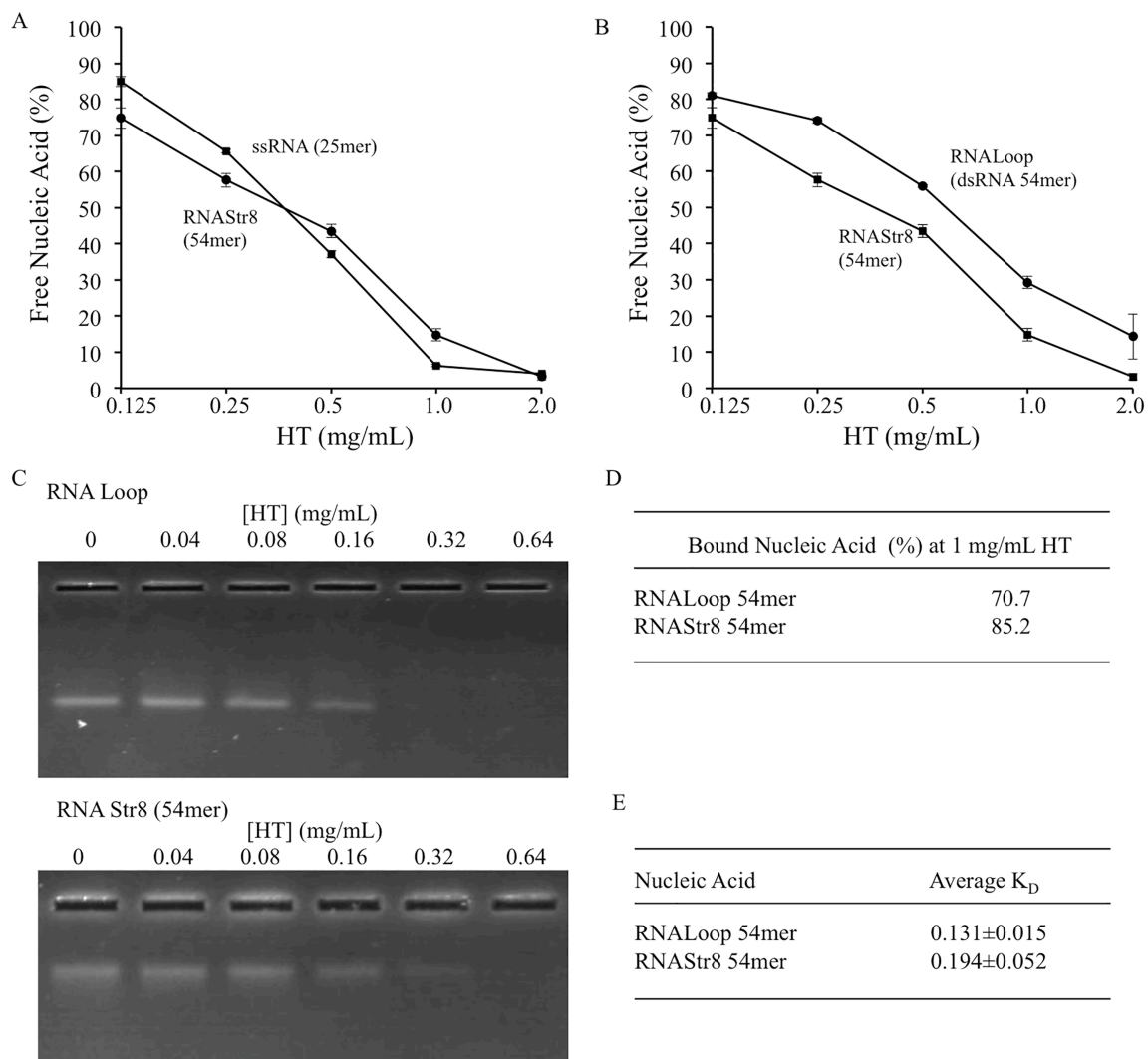


Fig 15. HT binding studies with RNALoop and RNAStr8 using centrifugation and electrophoretic mobility shift assays. (A) Comparison of free RNAStr8 vs. free ssRNA measured after binding to HT. (B) Comparison of free RNALoop dsRNA vs. dsRNA 25mer after binding to HT from centrifugation assays. (C) Electrophoretic mobility shift assays performed on RNALoop 54mers and RNAStr8 54mers with increasing HT concentrations. Top gel: *Lane 1*, RNALoop (100 ng); *lanes 2-6*, RNALoop (100 ng) + 0.04, 0.08, 0.16, 0.32, or 0.64 mg/mL HT, respectively. Bottom gel: *Lane 1*, RNAStr8 (150 ng); *lanes 2-6*, RNAStr8 (150 ng) + 0.04, 0.08, 0.16, 0.32, or 0.64 mg/mL HT, respectively. (D) RNALoop and RNAStr8 K_D data was found by performing densitometry analysis on EMSA gels using ImageJ software and generating a trendline equation in Microsoft Excel. Averages and standard deviations are shown.

In addition to assessing the interactions of HT with ssRNAs and dsRNAs, we also delved into investigating the binding affinity of HT for a more complex, 75-80 nt cloverleaf-like RNA molecule, tRNA (Figure 16). tRNAs participate in the translation of nucleic acids to proteins by recognizing the codons encoded in mRNA. Although they are not involved in the RNAi pathway, these RNAs were of interest to this study due to the possibility of single-stranded RNA molecules having intramolecular interactions that can result in complex stem-loop structures (49).

We performed centrifugation studies using a mixture of purified *E. coli* tRNAs (Sigma-Aldrich) and the same parameters that were used for the 25mers and 54mers. The data from the assays showed that up to 90% of tRNA binds to HT at both 1 mg/mL and 2 mg/mL HT concentrations (Figure 17A). Mobility shift assays for tRNA-HT resulted in an average K_D of 0.210 ± 0.006 (a representative gel is shown in Figure 17B). These data show that despite having a larger and more complex tertiary structure than the RNAs tested previously, tRNA has high affinity for HT. In fact, the amino acid acceptor end of the tRNA (the top end, Figure 16) is approximately 7.6 nm apart from the anticodon site (bottom end of tRNA molecule), with each arm being 2 nm in diameter (50, 52). Although the centrifugation and EMSA assays do not elucidate the mode of binding of tRNA to HT, it would be reasonable to assume that tRNA does not bind in the HT interlayer space based on X-ray diffraction analyses that have shown that the brucite spacing of HT is approximately 0.78 nm (7.8 Å) (51) and can only expand up to approximately 2.39 nm (23.9 Å) (53). However, it is not clear that this limitation is true for all hydrotalcites. The tRNA could therefore be adsorbing to the surface of HT. Conversely, because the tRNA stem-loops are 2 nm in diameter, they could be binding to

the edges of the interlayer space while the rest of the tRNA remains outside of the nanoparticle. Perhaps the other stem-loop/dsRNA portions of the tRNA could also become intercalated into other HT nanoparticles, causing HT to aggregate. In any case, one method to help resolve this question would be by performing X-ray diffraction on the tRNA-HT complexes to determine whether a change in the HT interlayer spacing is observed and if that change is consistent with the diameter of tRNA. Previous studies have suggested that dsDNA can intercalate into HT nanoparticles under some experimental conditions (Figure 18) (34).

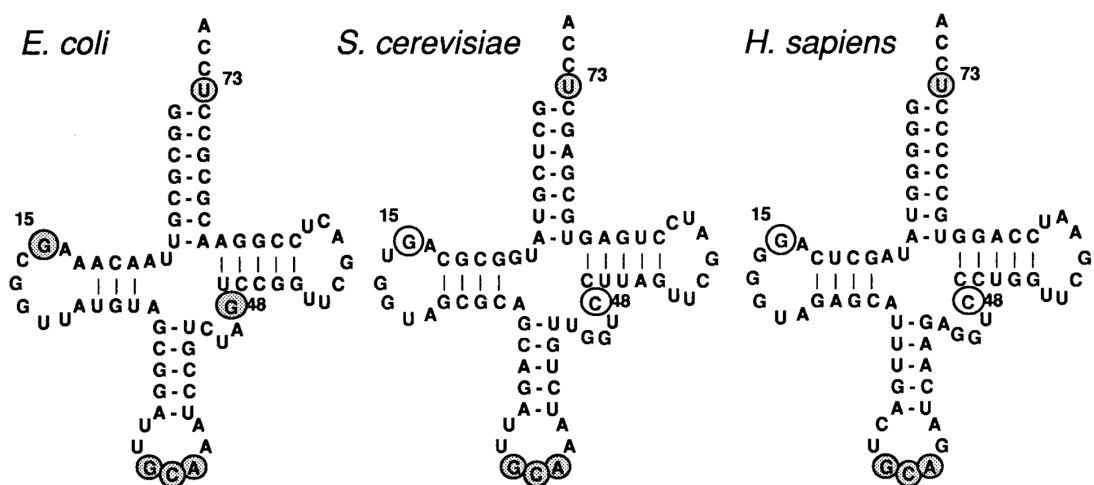


Fig 16. Examples of structures and sequences of *E. coli*, *S. cerevisiae*, and human tRNAs (52).

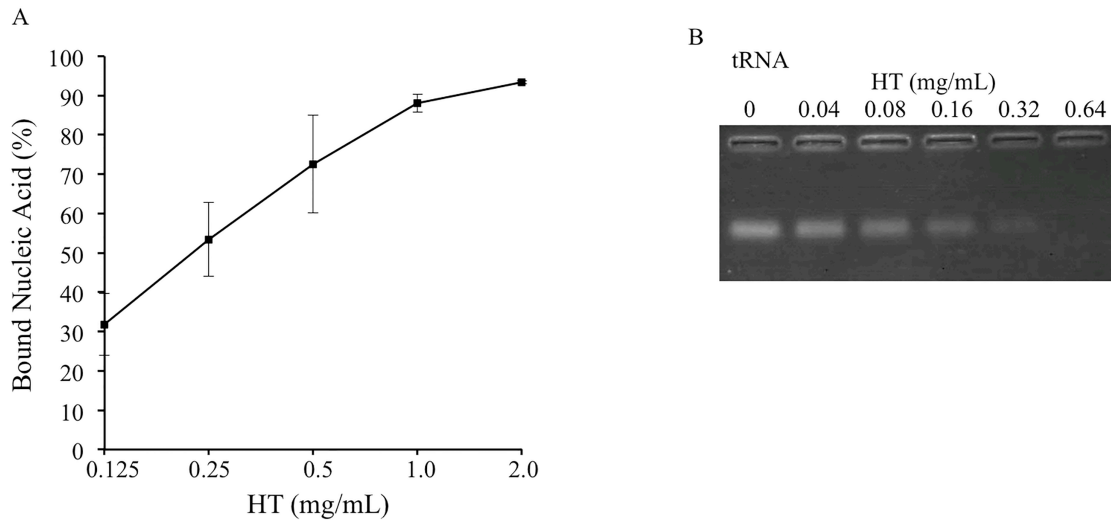


Fig 17. HT binding studies with tRNA using (A) centrifugation and (B) electrophoretic mobility shift assays.

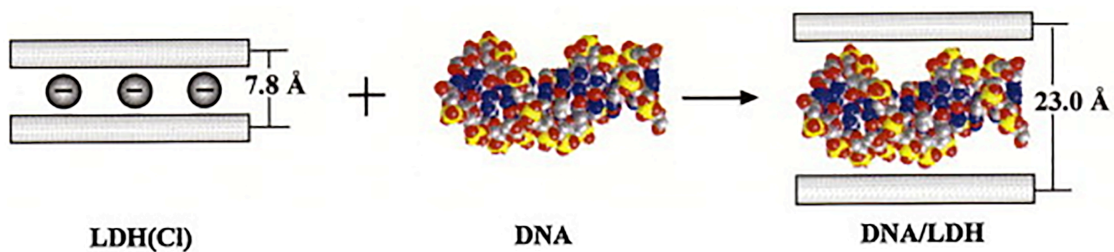


Fig 18. Schematic from Nakayama *et al.* showing the binding mode of DNA to HT from data collected by X-ray diffraction (34).

One of the attractive features of HT as a gene delivery carrier is its ability to exchange anions from the interlayer spacing. The HT that was used for the present study contained chlorine in the interlayer space, which was readily exchanged for nucleic acids. Interestingly, a study by Ishihara *et al.* (54) showed that when hydrotalcite containing CO_3^{2-} as the exchangeable anion is exposed to air, the anion can be exchanged with carbonate derived from atmospheric CO_2 (Figure 19). Ishihara *et al.* suggested that CO_2 most likely adsorbs to the Mg-OH site mediated by reversible acid-base interactions (54).

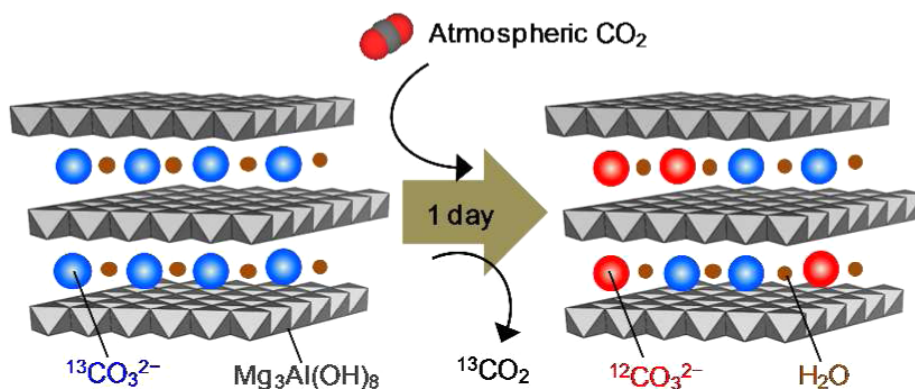


Fig 19. This schematic from Ishihara *et al.* shows that when HT is exposed to atmospheric air, the CO₂ can interact with the interlayer water and exchange the ¹³CO₃²⁻ for ¹²CO₃²⁻ (54).

Concern about anions displacing or competing off the RNA from binding to HT led us to conduct a series of centrifugation assays containing two distinct anions, sodium carbonate (Na₂CO₃), and sodium sulfate (Na₂SO₄). Competition assays were performed that involved simultaneously mixing 1 mg/mL HT with ssRNA 25mer (5 μM RNA; 125 μM phosphate) and increasing concentrations of sodium carbonate, or sodium sulfate at 1, 1, 10, or 500 mM. In Figure 20, the percentage of RNA remaining unbound in the presence and absence of other anions is plotted against the concentration of salt added. At the highest concentration, 500 mM, the amount of RNA bound to HT was reduced from 90-95% to ~50-60% using either salt (Figure 20A).

Displacement studies were performed in a similar manner, except that the anions were added last to the ssRNA-HT mixture, after RNA-HT complexes had already formed. Similar to the competition assays, at 500 mM anionic salt concentration, approximately 50% of the RNA bound initially was displaced from the HT (Figure 20B). There were, however, differences at 10 and 100 mM, with carbonate having the greatest impact at these concentrations. These experiments show that while anions such as

carbonate and sulfate can indeed be exchanged for RNA, the process is inefficient, even at very high concentrations of the anions.

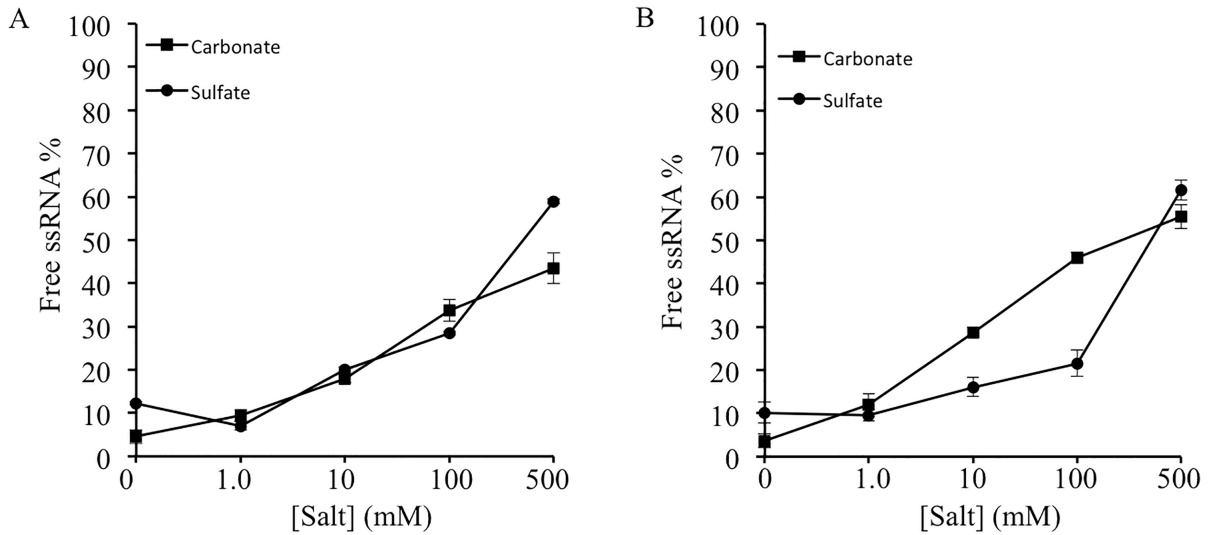


Figure 20. Centrifugation assays performed with ssRNA 25mers ($A_{260} \sim 1.0$), 1 mg/mL HT, and the addition of sodium carbonate (Na_2CO_3) or sodium sulfate (Na_2SO_4) at 0, 1, 10, 100, or 500 mM. (A) Centrifugation assays were performed to determine the ability of carbonate and sulfate to compete with ssRNA for HT binding. (B) Displacement of RNA from HT after adding carbonate and sulfate to the solution was also analyzed.

Numerous studies have focused on elucidating the role of homoionic montmorillonite in the origins of life as it has been shown to help catalyze the polymerization of RNA from activated mononucleotides (55-57). The interactions between RNA components and homoionic clay, in conjunction with findings that MMT can protect self-catalyzing RNA from degradation, have lent support to the hypothesis of the RNA World (56). Recently, montmorillonite has received attention for its ability to be involved in a completely different application. Similar to HT, montmorillonite has also been proposed as an effective gene delivery vehicle for drugs and DNA molecules. The interactions between MMT and DNA have been well documented in recent studies. Beall *et al.* reported intercalation of single-stranded DNA into MMT platelets by measuring the interlayer spacing of MMT after adsorption to ssDNA using X-ray diffraction (7). However, there has not been much focus on probing MMT as a carrier for RNA molecules for therapeutic purposes. Incorporating the fact that MMT can serve as a surface for RNA mononucleotides to promote polymerization and that it is capable of binding to and delivering DNA into cells, this study investigated the binding affinity of RNA molecules (Figure 11) for MMT.

The assays for the present study were conducted using different concentrations of the two most widely studied homoionic montmorillonite clays, Na-MMT and Ca-MMT (4-7, 9, 13, 14-22, 55-57). Modifying montmorillonite with cations is crucial for binding as the silica surface of MMT is negatively charged and would encounter electrostatic repulsion to the negatively charged RNA and DNA. Moreover, reports have shown that binding of nucleic acids to MMT can be promoted by the addition of salts such as NaCl and MgCl₂ (8, 16, 55); therefore, assays were performed with and without the addition of

salts. Both Na-MMT and Ca-MMT were sonicated for 4 minutes before use to allow the tactoids of clay platelets to disperse. Sonication of MMT is important when binding to biomolecules as it increases the available surface area to which biomolecules can bind and has been proposed as an essential step in preparing MMT that can intercalate DNA (7).

The design of the adsorption experiments was similar to the HT-RNA centrifugation assays. As Beall *et al.* reported in their studies, in order to obtain accurate 260 nm absorbances, it is necessary to account for the A_{260} contributions of MMT (7). The centrifugation assays, therefore, consisted of an additional set of control tubes (Figure 21A). These tubes contained MMT at 0.2, 0.5, 1.25, or 3.125 mg/mL and water only. After centrifugation, the A_{260} of the supernatant of each tube containing MMT only was measured using a spectrophotometer and was subtracted from the A_{260} measured from the supernatant of each tube containing the same concentration of MMT plus RNA, to obtain the absorbance of free nucleic acids (Figure 21B). While a 5 min spin at 21,000 x g was sufficient to sediment the HT nanoparticles and separate them from the unbound oligonucleotides (Figure 10), MMT assays required a harder and longer spin (25,000 x g for 1 h) (data not shown). It was also imperative to increase the amount of RNA used for these assays to an A_{260} of 1.0, in order to help offset the background MMT A_{260} contributions.

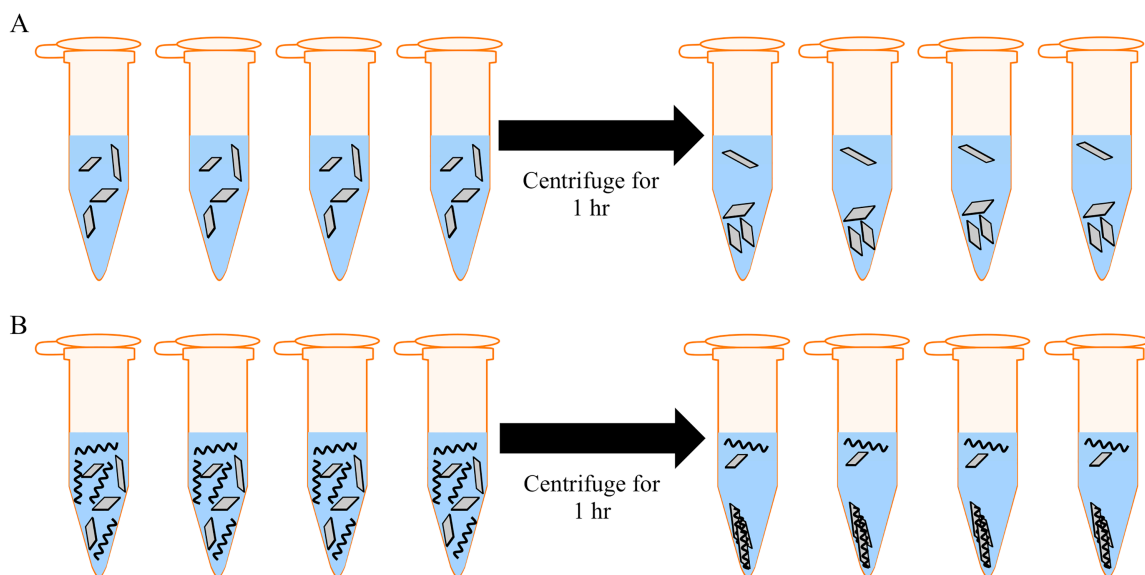


Fig 21. RNA-MMT centrifugation assays. (A) Control tubes contained MMT (0.2, 0.5, 1.25, 3.125 mg/mL) and ddH₂O. (B) RNA ($A_{260} = 1$) was mixed with MMT (0.2, 0.5, 1.25, 3.125 mg/mL) and ddH₂O. Sedimented MMT with bound RNA formed a pellet after a 1 h spin at 25,000 x g. Unbound RNA and a small amount of MMT remained in solution.

The ability of 25mers to bind to Na-MMT was evaluated using centrifugation studies. The results are presented in Figure 22, in which the free, or unbound, RNA or DNA is plotted against increasing concentrations of Na-MMT. Again, ssDNA and dsDNA were included in these assays in order to maintain an internally controlled study with the knowledge that DNA is known to bind to MMT and to intercalate under some conditions. No significant binding occurred between the 25mers and Na-MMT without the addition of salts (Figure 22A). Assays using ssRNA, ssDNA, and dsDNA 25mers consistently resulted in > 90% of nucleic acids remaining unbound, even at the highest Na-MMT concentration (3.125 mg/mL), and results with the dsRNA 25mer were similar (83% - 92%) (Figure 22A). These data show that despite the overall positive charge from the sodium ions on Na-MMT, this monovalent cation was not sufficient to mediate the adsorption between MMT and nucleic acids.

The effect of NaCl and MgCl₂ on binding of nucleic acids to Na-MMT was tested by mixing 0, 0.1, 1, and 10 mM NaCl or MgCl₂ with 0.5 mg/mL Na-MMT and ssDNA, ssRNA, dsDNA, or dsRNA 25mers. The addition of NaCl had no detectable effect on the amount of unbound RNA and DNA (Figure 22B). On the other hand, the addition of MgCl₂ significantly promoted the adsorption of the nucleic acids to Na-MMT. ssRNA and ssDNA bound strongly when MgCl₂ was raised to 10 and 100 mM (75-95% bound, corresponding to 5-25% free nucleic acid in Figure 22C). In contrast, binding of dsRNA and dsDNA was increased in the presence of MgCl₂, but only achieved 30-55% binding at 10 mM and 100 mM MgCl₂. It has been established that Na-MMT has high affinity for DNA 25mers in the presence of salts (7, 56), and our internally controlled experiments show that RNA 25mers share adsorption characteristics with DNA 25mers (Figures 22A, 22D).

Overall, these results suggest that 25mers have little to no adsorption to Na-MMT, but the addition of salts, in particular MgCl₂ at 10 mM or higher, drastically improves the adsorption of the RNA and DNA to Na-MMT. ssRNA 25mers adsorbed to 0.5 mg/mL Na-MMT approximately 2-fold more strongly than dsRNAs, in the presence of 10 and 100 mM MgCl₂ (Figure 22C).

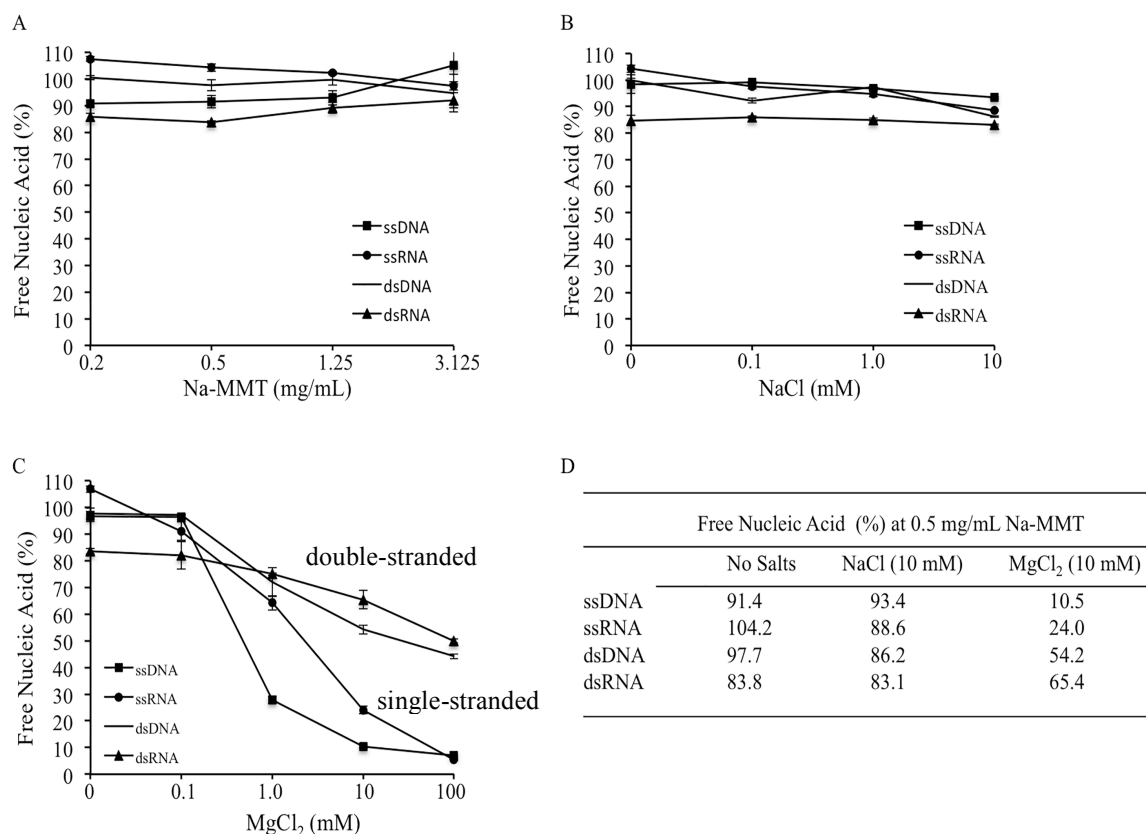


Fig 22. Na-MMT centrifugation assays with ssDNA, ssRNA, dsDNA, and dsRNA 25mers. (A) Binding of four nucleic acids to increasing concentrations of Na-MMT (B and C) Impact of adding NaCl and MgCl₂ on binding of nucleic acids to 0.5 mg/mL clay. (D) Percentage of free nucleic acids in the supernatant with and without 10 mM NaCl or 10 mM MgCl₂.

The addition of divalent cations enhances the interactions between nucleic acids and Na-MMT by providing strong electrostatic interactions between the negatively charged phosphate backbone of the nucleic acids and the negatively charged silica layer (15, 55). Interactions between anionic polymers and clay have widely been speculated to occur via cation bridging (Figure 23) (55). This model illustrates the role of cations in mediating the interactions between the negatively charged phosphate backbone of the nucleic acids and the negative charge of the silica layer in MMT. It can also explain why single-stranded 25mers bind twice as well to MMT as double-stranded 25mers. The

charge density of double-stranded nucleic acids is twice as much as the single-stranded nucleic acids, and as a result, a higher concentration of cations would be required to offset the repulsion from the negatively charged nucleic acids to the anionic MMT surface.

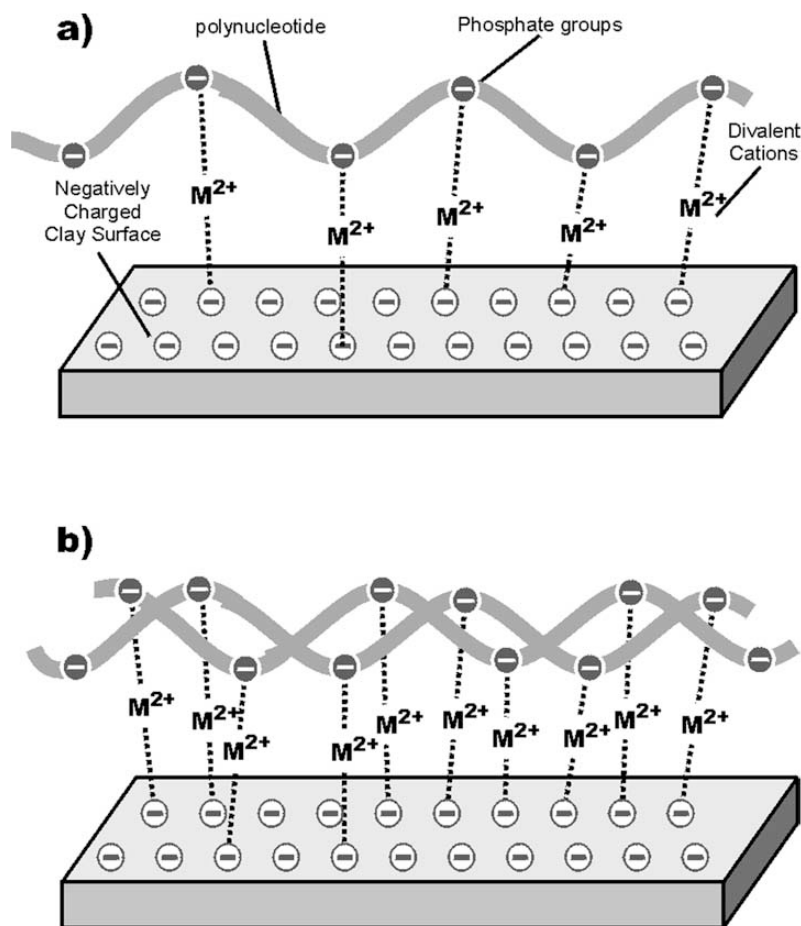


Fig 23. Proposed cation bridging model by Franchi *et al.* illustrates the role of divalent cations during binding of MMT with (A) single-stranded oligonucleotides and (B) double-stranded oligonucleotides at pH > 5 (55).

Three different ways cations can interact with RNA anions in aqueous solutions are represented in Figure 24. The three exchangeable cations used in this study, Na^+ , Ca^{+2} and Mg^{+2} , form cation bridges in the interlayer MMT spacing by coordinating outer-sphere complexes with siloxane surfaces (Figure 23 and Figure 24) (58). The interlayer

swelling of MMT is a key feature in accommodating nucleic acids into the interlayer space. Na *et al.* employed molecular dynamics to investigate the properties of MMT interlayer spacing in relation to the water content and the type of cation present (59). They found that the presence of Mg^{2+} in Na-MMT helps increase the interlayer spacing at high water content. This could potentially affect the ability of nucleic acids to intercalate between MMT sheets and could be a contributing factor in the interactions between 25mers and Na-MMT. An assumption could be made on the basis that the presence of magnesium not only serves as a counterion to form cation bridges with the RNA-MMT, but that it also interacts with the RNA molecules and stabilizes their structure. This could imply that without the support of stabilizing ions, perhaps the RNA molecules form secondary structures, reducing their ability to intercalate between the MMT sheets. This could go hand-in-hand with the fact that ssRNA has a 2-fold greater adsorption to Na-MMT than the dsRNA and could indicate that the extended linear structure of ssRNA can bind in the interlayer space to Mg^{2+} with more ease than dsRNA because of its conformation. The validity of this argument was tested further.

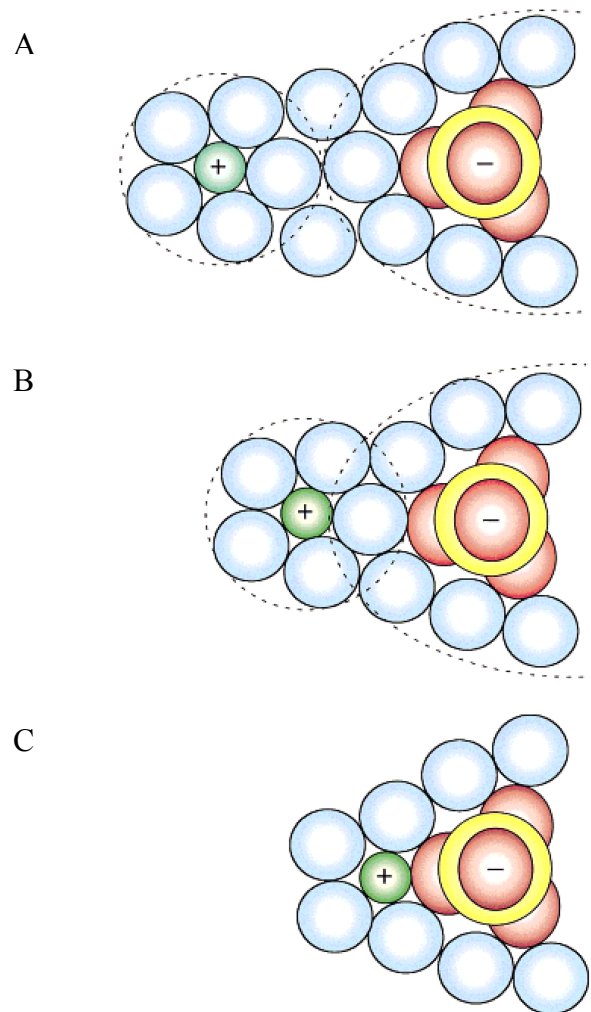


Fig 24. Representation of the binding modes between RNA and magnesium as depicted by Misra and Draper (60). (A) Non-specific interactions occur between magnesium and the phosphate of RNA by which the solvation shell of each molecule is separate from one another; (B) the solvation shell of RNA and magnesium overlap, this binding mode is typically referred to as the outer-sphere complex; (C) this inner-sphere complex involves the direct interaction of RNA and a cation in a dehydrated binding site.

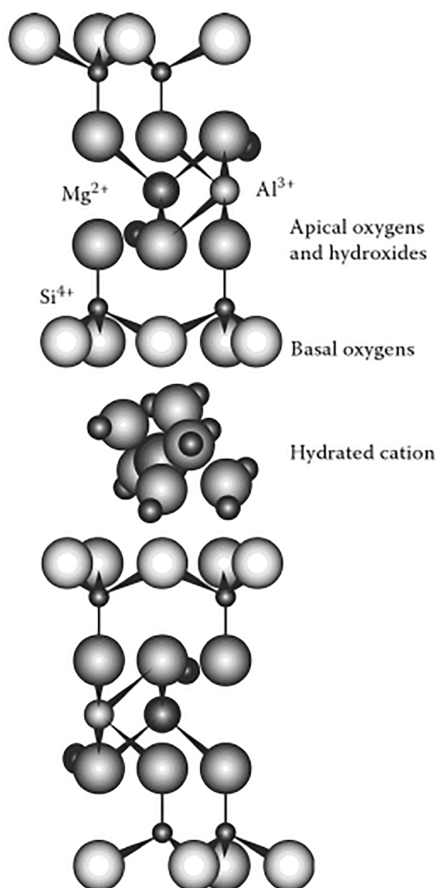


Fig 25. This figure from Essington M. E. shows an example of outer-sphere complexation between the montmorillonite siloxane surface and a hydrated cation (58).

Following the HT-RNA experimental protocol described earlier, the adsorption of two 54mers (RNAstr8 and RNALoop) (Figure 11) to Na-MMT with and without the presence of NaCl or MgCl₂ was assayed. The results of these centrifugation studies are shown in Figure 26. No adsorption occurred between the RNAstr8 54mer and Na-MMT, while the RNALoop 54mer exhibited slight affinity for Na-MMT (15.6%, 24.2%, and 35.8% bound at 0.5 mg/mL, 1.25 mg/mL, and 3.125 mg/mL Na-MMT, respectively) (Figure 26A).

Adding increasing amounts of NaCl to the Na-MMT/RNA mixtures had no significant effect on the adsorption of either RNALoop or RNAstr8 to 0.5 mg/mL Na-

MMT (Figure 26B). As with the 25mers, $MgCl_2$ promoted adsorption of the RNA 54mers strongly. Notably, 87.3% of the RNAStr8 adsorbed to Na-MMT at 10 mM $MgCl_2$ and even reached 100% adsorption at 100 mM $MgCl_2$ (Figure 26C). In contrast, only 35.8% and 43.5% of RNALoop adsorbed to Na-MMT at 10 and 100 mM $MgCl_2$. Again, a 2-fold difference in adsorption between a single-stranded RNA and an RNA with double-stranded character was observed (Figure 26D). The enhanced adsorption of RNA with the addition of Mg^{2+} occurred through a linear dependence of the concentration of magnesium present in solution, which demonstrates that adsorption depends on the type of cation and the concentration of the exchangeable cations.

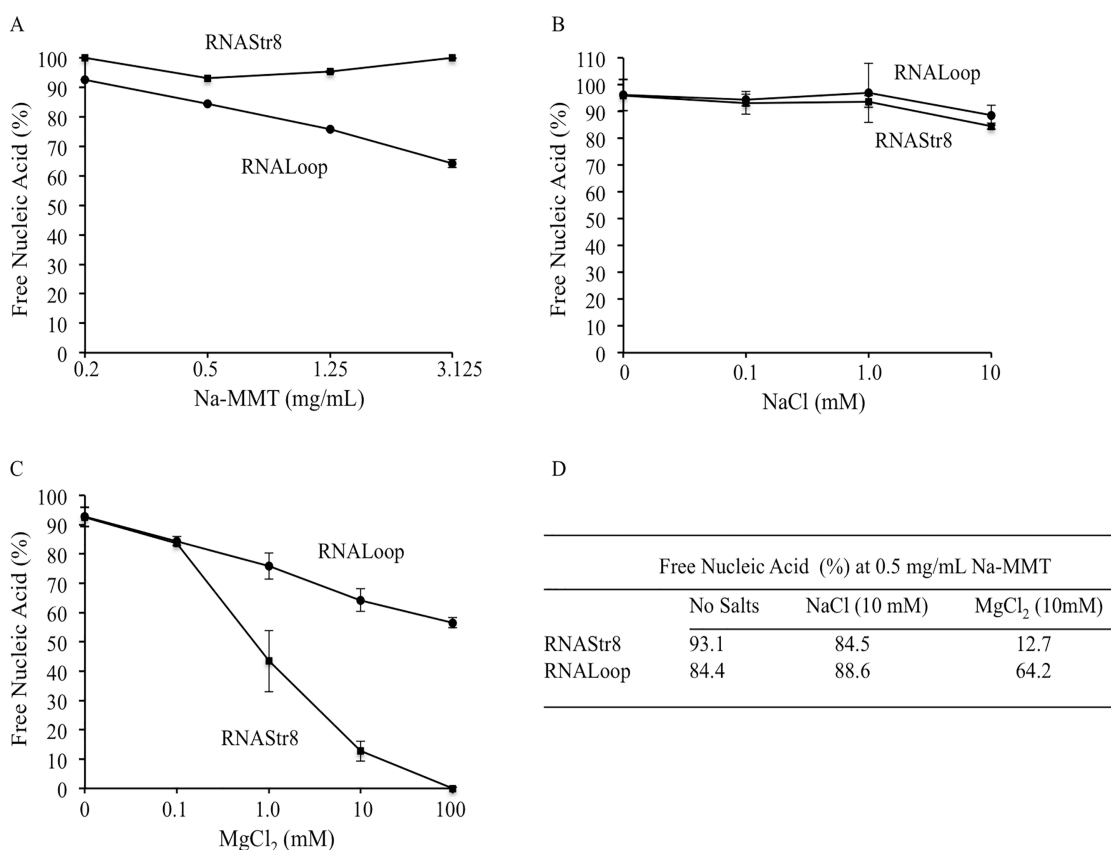


Fig 26. Adsorption assays using RNAStr8 and RNALoop with Na-MMT. The percentage of RNA remaining in the supernatant after centrifugation is shown in (A). The effect of clay concentration on RNA binding. (B and C) Impact of adding either NaCl or $MgCl_2$ on binding of RNA to 0.5 mg/mL clay. (D) Comparison of the free RNAStr8 and RNALoop % at 0.5 mg/mL Na-MMT without and in the presence of NaCl or $MgCl_2$.

These results, contrary to the hypothesis that the overall charge density of RNA is a determining factor in adsorption to Na-MMT, show that it must not be essential given the fact that both RNAStr8 and RNALoop possess a potential -54 overall charge yet a 2-fold difference in adsorption was observed. It can be assumed that RNA structure plays a critical role in the interactions between Na-MMT and RNA, whereby the clay preferentially binds to single-stranded RNAs over the double-stranded RNAs. Although the predominant form of interaction between nucleic acids and MMT is likely to occur through cation bridging within the interlayer spacing, there is a possibility that the nucleic acids can also adsorb to MMT on the surface edges or by tactoid exfoliation (Figure 27B and 27C). The adsorption of anionic polymers on MMT edge surfaces can be explained by specific ligand-exchange interactions between the phosphate groups of DNA to the hydroxyl of groups on the montmorillonite. It would be of interest to determine the dominant mode of interaction between Na-MMT and the 54mers by performing X-ray diffraction, SEM microscopy, or by blocking the edge surfaces by treating the clay with sodium tripolysphosphate (56). A study by Lin *et al.* showed that modifying montmorillonite with hexadecyltrimethylammonium expanded the interlayer gallery, allowing double-stranded DNA molecules to intercalate (18). Expanding on this approach with RNALoop and RNAStr8 could provide interesting data on the significance of having a more accessible interlayer gallery.

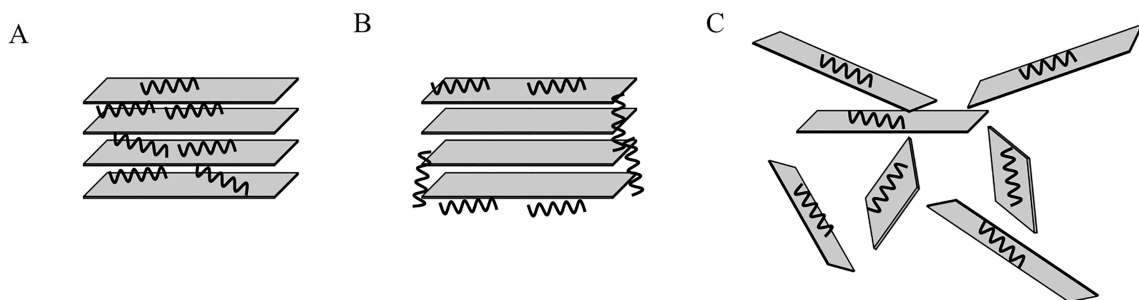


Fig 27. Proposed modes of interaction between nucleic acids and montmorillonite include (A) intercalation between sheet platelets, (B) binding to the surface or edges of MMT, or (C) tactoid exfoliation upon adsorption.

The adsorption of tRNAs on Na-MMT in the absence and presence of NaCl and MgCl₂ was also assessed. Without adding cations, no adsorption to Na-MMT was observed (Figure 28A). Although NaCl had no effect, addition of MgCl₂ enhanced binding at 1 mM and 10 mM concentrations (Figure 28B). At 1 mM MgCl₂, 84.5% of tRNA was unbound, at 10 mM MgCl₂, 72.3% was unbound, and at 100 mM MgCl₂, 67.2% remained unbound (100 mM data not shown in Figure 28). This indicates that Na-MMT has low affinity for tRNAs. It has been established that cations such as Na⁺ and Mg²⁺ are important for stabilizing the tertiary structure of tRNA (60). This could be an important contributing factor to tRNA maintaining its structure after adsorption to MMT. However, it could also be the reason why little adsorption was observed between tRNA and Na-MMT, even with the addition of MgCl₂. Perhaps the complex tRNA structure is unable to fit into the interlayer galleries due to steric hindrance. The question concerning the ability of tRNA to be accommodated into the MMT interlayer remains unanswered without structural studies. While it remains to be seen if tRNA intercalates between MMT platelets, the same mode of binding that was proposed for the tRNA binding to HT could be occurring here. As previously mentioned, the phosphate groups of RNA can bind to

the hydroxyl groups on the surface edges of MMT. This could potentially be one of the modes of adsorption. Another mode could be that tRNA binds to the outer surface of the MMT sheets, mediated by cation bridging.

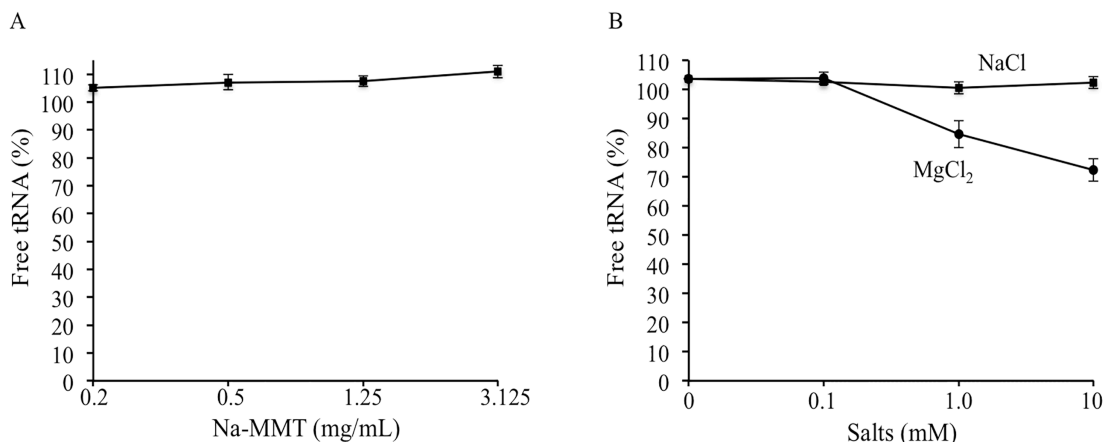


Fig 28. tRNA adsorption assays using Na-MMT with and without the addition of NaCl or MgCl₂.

The next set of experiments consisted of using Ca-MMT as the homoionic clay for the RNA adsorption assays. Due to the ability of divalent cations to promote clay-nucleic acids interactions via cation bridging (7), these assays were expected to yield quite different results than the Na-MMT assays. For example, bridging could occur even without the addition of MgCl₂, as the clay would already have divalent cations bound to the negative silica layer. Not only that, but Ca²⁺ is known to form inner-sphere complexes with DNA, unlike Na⁺, which can only screen the negative charges through cation bridging (61). This could be important in the formation of strong interactions between the calcium ions and the nucleic acids. Indeed, Figure 29A shows that RNA 25mers and 54mers bind to Ca-MMT without the addition of salts. Notably, single-stranded RNAs (ssRNA 25mer and RNAStr8) reached 70-80% binding to Ca-MMT at 3.125 mg/mL. In agreement with the Na-MMT assays in the present study, dsRNA and RNALoop

exhibited an approximately 2-fold adsorption decrease compared to their single-stranded counterparts (Figure 29A). When increasing amounts of $MgCl_2$ were added to the assays using 0.5 mg/mL Ca-MMT, adsorption was only moderately increased for the 25mers and 54mers (Figure 29B).

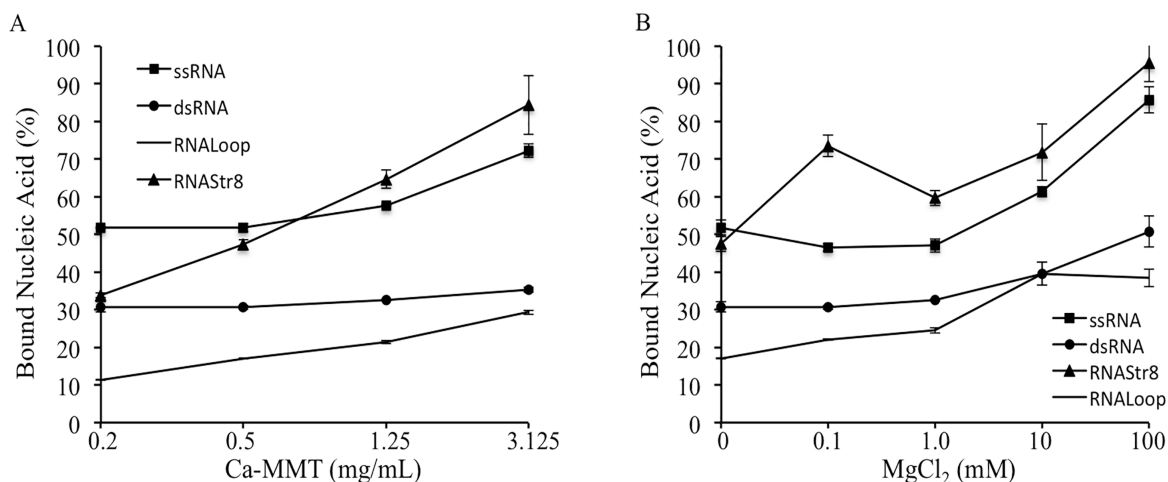


Fig 29. Adsorption assays involving 25mers and Ca-MMT. (B) The 25mers were also assayed for their adsorption to Ca-MMT in the presence of $MgCl_2$.

Another possible contributing factor to explain why nucleic acids adsorb twice as much on Ca-MMT clays and on clays with $MgCl_2$ in the solution, is the smaller ion size and hydration energy of Na^+ ions when compared to calcium or magnesium. Na^+ ions are not able to open up the interlayer space of MMT to the same extent that divalent cations can, thereby retaining fewer H_2O molecules in the interlayer space (62). A decrease in H_2O content can cause the interlayers to collapse (62). This would suggest that nucleic acids are limited in accessing the interlayer space when sodium is the exchangeable cation.

These data demonstrate that, while divalent cations are key to promoting binding between RNA 25mers and 54mers, they have a greater impact when added to Na-MMT

than Ca-MMT. In fact, 0.5 mg/mL Na-MMT + MgCl₂ adsorption assays showed greater adsorption for ssRNA, RNAStr8 and dsRNA than 0.5 mg/mL Ca-MMT assays (without added salts). This could be due to reduced available surface area due to the tactoid formation that occurs in Ca-MMT, which is not as prevalent in Na-MMT. Despite sonicating the Ca-MMT clay, some tactoids still remain, thereby precluding a substantial number of RNAs from intercalating between MMT platelets.

The last set of MMT centrifugation assays were between tRNAs and Ca-MMT with or without the presence of MgCl₂. Addition of increasing amounts of the clay in water produced only 20% - 40% binding of the tRNAs (Figure 30A), similar to the dsRNAs in Figure 29A. Greatest binding was achieved (~40%) at the highest Ca-MMT concentration (3.125 mg/mL). Bound tRNA was at 32.8% with 0.5 mg/mL Ca-MMT at 100 mM MgCl₂ (Figure 30B). The adsorption onto Na-MMT at the same MgCl₂ concentration was 30.9%, indicating that there was no difference between salt studies of Na-MMT and Ca-MMT (Figure 30). It appears that the highest adsorption occurred at the highest Mg⁺² concentration and the highest Ca²⁺ concentration, highlighting the similarity between divalent cations in promoting binding.

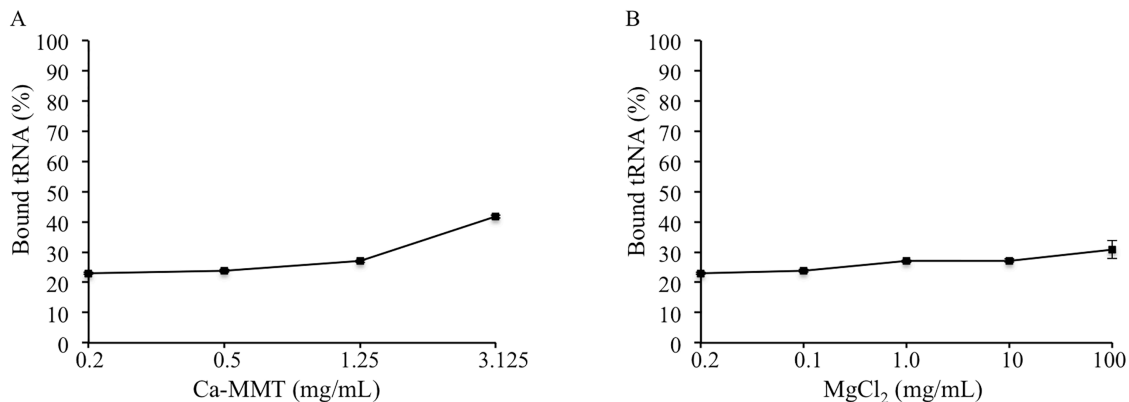


Fig 30. tRNA adsorption to Ca-MMT was assayed. (B) tRNA adsorption was also assayed in the presence of MgCl₂.

The next logical step was to assess the binding of RNA to MMT by performing electrophoretic mobility shift assays similar to the RNA-HT EMSAs. When dealing with MMT, however, there were considerations that had to be taken into account. For instance, the buffer of choice for the RNA-HT EMSAs was 0.5X TB (Tris and boric acid). When we ran a pilot gel of ssRNA 25mer (200 ng) with increasing concentrations of Ca-MMT (0, 0.2, 0.5, 1.25, 3.125 mg/mL) no shift in the free RNA band was observed (Figure 31A). The reasoning behind using Ca-MMT and ssRNA was that on the basis of the centrifugation assays, ssRNA and Ca-MMT (without the addition of salts) showed high adsorption.

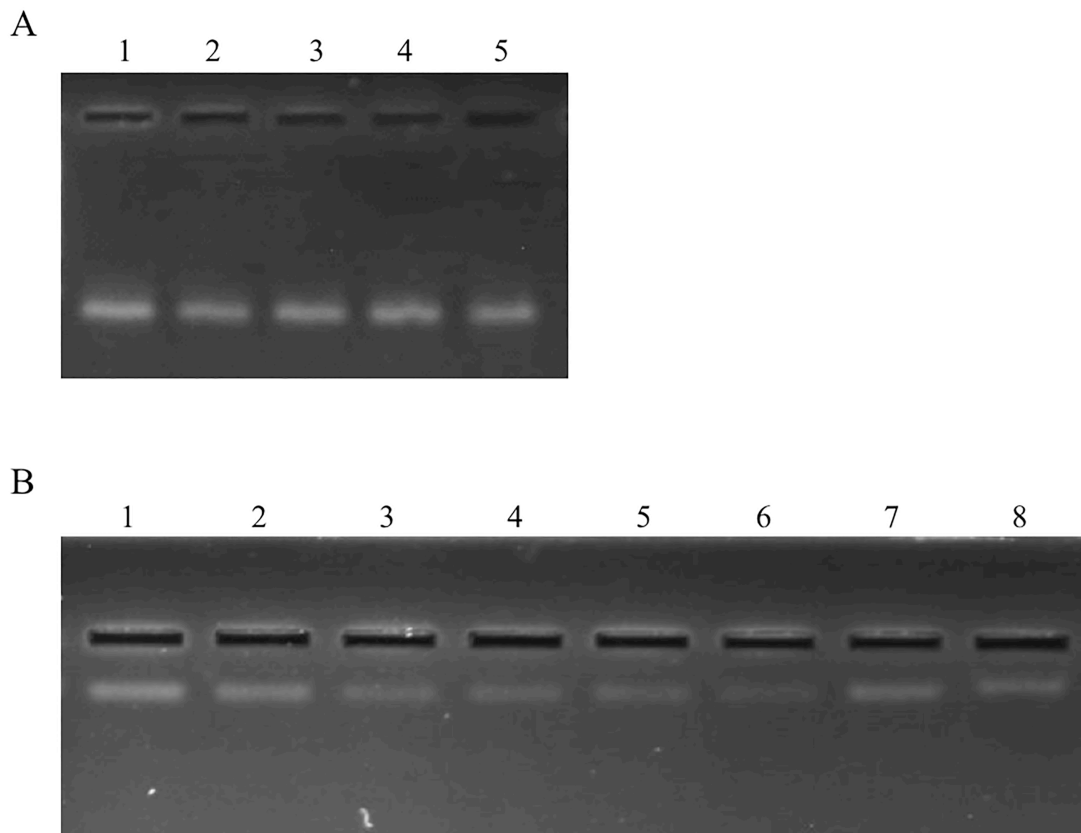


Fig 31. Electrophoretic mobility shift assays performed on ssRNA 25mers with increasing HT concentrations. (A) *Lane 1*, ssRNA (200 ng); *lanes 2-5*, ssRNA (200 ng) + 0.04, 1, 2.5, and 5 mg/mL Ca-MMT, respectively. (B) *Lane 1*, ssRNA (150 ng); *lanes 2-5*, ssRNA (150 ng) + 1, 2.5, and 5 mg/mL Ca-MMT, respectively; *lane 6*, ssRNA + 1 mg/mL Ca-MMT + 10 mM MgCl₂; *lane 7*, ssRNA + 2.5 mg/mL Ca-MMT + 10 mM MgCl₂; *lane 8*, ssRNA + 0.5 mg/mL Na-MMT + 10 mM MgCl₂; *lane 9*, ssRNA + 0.5 mg/mL Na-MMT + 100 mM MgCl₂.

It is not clear why the bound complexes did not appear as shifted bands in the EMSA assay. Prior reports have shown that MMT is able to adsorb to both Tris and boric acid (63-64). Sakie *et al.* found that Tris can act as a bridge between DNA and montmorillonite, albeit a weak one in comparison the cation bridge by divalent cations such as Ca²⁺ (63). They outlined two possible scenarios (Figure 32) to help explain how this bridging can occur (63). Essentially, because the pH of Tris is typically lower than its

pKa, most of the NH_2 groups will become positively charged into NH_3^+ . The positively charged Tris-NH_3^+ molecules would then bind to the negatively charged silicate layer while the OH groups on Tris would interact by hydrogen bonds with the DNA backbone (Figure 32i). Alternatively, the $-\text{NH}_3^+$ group could interact directly with the DNA and the $-\text{OH}$ groups could interact with the montmorillonite surface (Figure 32ii) (63). Although the specific mechanism by which Tris might bridge the interactions between nucleic acids and MMT has not been elucidated, these EMSAs suggest that it may interfere with such assays.

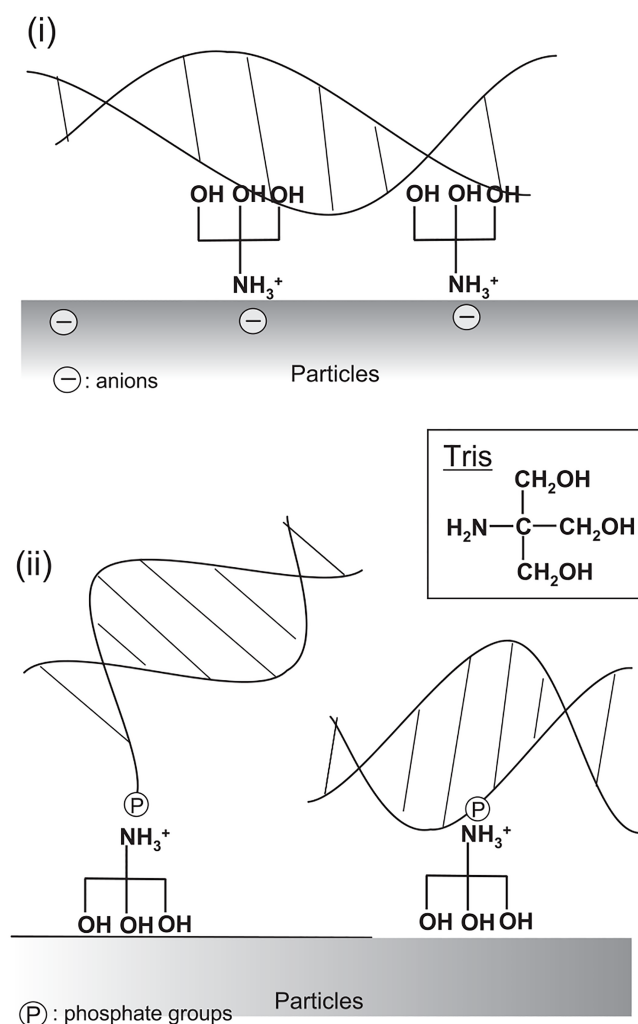


Fig 32. Conceptual schematic from Saeki *et al.* illustrating the possible ways Tris interacts with DNA molecules and montmorillonite (63).

Boric acid from 0.5X TB buffer may also pose a potential problem. According to Keren and O'Connor, anionic boric acid can be adsorbed to the surface of montmorillonite through a ligand exchange mechanism, in which the boric acid can displace water or hydroxides from the montmorillonite surface and bind to the Na or Ca cations of homoionic MMT (64). Therefore, we opted to test another electrophoresis running buffer that does not include Tris or boric acid.

To substitute for 0.5X TB, 1X Tricine/Triethanolamine (65) was tested. As shown in Figure 31B, lanes 2, 3, 4, and 5, with this buffer there was a gradual decrease in band intensity with increasing Ca-MMT concentration. However, at no point did the free RNA band disappear, even at the high 5.0 mg/mL concentration. Experiments were performed that involved running the gel for only 5 min in an attempt to minimize dissociation of the clay and the RNA. We also ran samples containing ssRNA (150 ng) and Ca-MMT supplemented with 10 mM MgCl₂, as well as samples containing 0.5 mg/mL Na-MMT supplemented with 10 or 100 mM MgCl₂ (Figure 31B, lanes 6, 7, and 8). Inclusion of MgCl₂ was based on the adsorption studies that showed high interaction between ssRNA and 0.5 mg/mL Na-MMT in the presence of 10 and 100 mM MgCl₂. No strong interactions were observed in any of the gels. Because of the inability to detect binding in EMSAs run with RNA and MMT, this type of binding data could not be compared with the data from the centrifugation assays as it was done for HT. Optimization will be required in order to be able to use EMSAs effectively to quantitate the binding affinity of RNA molecules to montmorillonite.

CHAPTER IV

SUMMARY AND CONCLUSIONS

The purpose of this study was to analyze the binding affinities of different RNA molecules for hydrotalcite and montmorillonite. Experiments with HT demonstrated that using a simple ion-exchange by centrifugation is a reliable method to measure binding of RNAs, as hydrotalcite sediments exceptionally well and does not contribute to the A_{260} measurements of free RNA.

The centrifugation assays showed that small RNAs and small DNAs bind similarly to HT. A 2-fold difference in binding was apparent between ssRNA and dsRNA, where ssRNA had the greater affinity for HT, and similar results were seen with ssDNA and dsDNA. Electrophoretic mobility shift assays confirmed this 2-fold difference.

The 54mers, RNAStr8 (ssRNA) and RNALoop (dsRNA) were assayed for their binding affinity for HT. Centrifugation studies revealed that no significant difference in adsorption occurred between RNAStr8 and RNALoop. Additionally, when comparing the 54mer to 25mer adsorption data, it was clear that the increase in overall charge density of RNA oligonucleotides was not a significant factor in determining adsorption efficiency to hydrotalcite. EMSAs also showed that the affinity for hydrotalcite did not differ between single-stranded vs. double-stranded RNA 54mers. It remains unclear why ss 25mers consistently bound HT 2-fold better than ds 25mers, but ss and ds 54mers bound with similar affinities.

Centrifugation and mobility shift assays indicated that tRNA has high affinity for HT, despite having complex tertiary structure, as well as the largest overall charge

density of the molecules tested here. These results could be expanded on by performing structural studies that would inform on the mechanism of interaction between the different RNA molecules and hydrotalcite. Being able to differentiate between RNA molecules that can intercalate in HT from RNA molecules that bind on the surface or edges could help to explain the results from this study. This study also provided evidence that high concentrations of carbonate or sulfate ions can replace RNA molecules. However, RNA was not easily displaced or competed off from the interlayer space.

Adsorption studies were also performed using RNA molecules and homoionic montmorillonite. High adsorption was observed for single-stranded and double-stranded 25mers and 54mers on Na-MMT in the presence of Mg^{2+} . A 2-fold greater adsorption was observed for single-stranded molecules compared to the double-stranded molecules. However, 54mers showed similar adsorption to 25mers. This result is at odds with the cation-bridging mechanism, which emphasizes the importance of charge density for adsorption to clay. While cation bridging could be mediating the interaction between RNA molecules in order for them to intercalate into MMT, other mechanisms of binding could also be at play. Despite the differences in charge density, the high affinity of Na-MMT+ $MgCl_2$ for ssRNA could be due to its structure and its ability to intercalate easier into Na-MMT sheets than dsRNA molecules. A low percentage of tRNA molecules bound to Na-MMT, even with the addition of $MgCl_2$, indicating low affinity of tRNA for the sodium clay. Assays performed on ssRNA, dsRNA, RNALoop and RNAStr8 using Ca-MMT showed a 2-fold greater affinity of single-stranded RNAs compared to the double-stranded RNAs. Addition of $MgCl_2$ did not result in a significant difference in adsorption of 25mers and 54mers to Ca-MMT, possibly due to calcium being a divalent

cation. tRNA also showed low affinity for Ca-MMT. Future studies might include using Fourier transform infrared spectroscopy and circular dichroism to determine if upon binding to nanoclays, the RNA molecules retain their conformation. These studies would be particularly interesting for tRNA – MMT assays.

Attempts to assess the binding affinity of RNA molecules to Na-MMT and Ca-MMT using electrophoretic mobility shift assays were unsuccessful, possibly due to the fact that Tris and boric acid interact with MMT. It is necessary to ensure that MMT does not interact with buffers used in the EMSAs, which could interfere with the binding between RNA and MMT. Results were slightly improved using an alternate buffer, but further optimization is required.

REFERENCES

1. Sokolova, V.; and Epple, M. *Angew Chem.* **2008.** 47, 1382 – 1395.
2. Wilczewska, A. Z.; Niemirowicz, K.; Markiewicz, K. H.; and Car, H. *Pharmacol Rep.* **2012.** 64, 1020-1037.
3. De Jong, W. H.; and Borm, P. J. A. *Int J Nanomedicine.* **2008.** 3, 133-149.
4. Suresh, R.; Borkar, S. N.; Sawant, V. A. Shende, V. S.; and Dimble, S. K. *Int J Pharm Sci Nanotechnol.* **2010.** 3, 901 – 905.
5. Choy, J. H.; Choi, S. J.; Oh, J.; and Park, T. *Appl Clay Sci.* **2006.** 36, 122 – 132.
6. Aguzzi, C.; Cerezo, P.; Viseras, C.; and Caramella, C. *Appl Clay Sci.* **2006.** 36, 22-36.
7. Beall, G. W.; Sowersby, D. S.; Roberts, R. D.; Robson, M. H.; and L. K. Lewis. *Biomacromolecules.* **2009.** 10, 105-112.
8. Sanderson, B. A.; Sowersby, D. S.; Crosby, S.; Goss, M.; Lewis, L. K.; and Beall, G. W. *Biointerphases.* **2013.** 8, 8.
9. Lin, F.; Chen, C.; Cheng, W. T. K.; and Kuo. *Biomaterials.* **2006.** 27, 3333-3338.
10. Pusch, R. and Yong; R. N. *Spon Research, CRC Press.* **2006.**
11. Cadene, A.; Durand-Vidal, S.; Turq, P.; and Brendle, J. *J Colloid Interface Sci.* **2005.** 285 (2), 719-730.
12. Helmy, A. K.; Ferreira, E. A.; and Bussetti, S.G. *J Colloid Interface Sci.* **1999.** 210, 167-171.
13. Lal, R. *Encyclopedia of Soil Science.* **2006.** 1, 277.
14. Winter, D.; and Zubay, G. *Orig Life Evol Biosph.* **1995.** 25, 61-81.
15. Soil colloids and the Surface Chemistry of soils <
http://faculty.yc.edu/ycfaculty/ags105/week08/soil_colloids/soil_colloids_print.html>
16. Cai, P.; Huang, Q.; and Zhang, X. *Appl Clay Sci.* **2006.** 32, 147-152.
17. Hou, Y.; Wu, P.; and Zhu, N. *Chemosphere.* **2013.** 95, 206-212.
18. Lin, F. H.; Lee, Y. H.; Jian, C. H.; Wong, J.; Shieh, M.; and Wang, C. *Biomaterials.* **2002.** 23, 1981-1987.

19. Kawase, M.; Hayashi, Y.; Kinoshita, F.; Yamato, E.; Miyazaki, J.; Yamakawa, J.; Ishida, T.; Tamura, M.; and K. Yagi. *Biol Pharm Bull.* **2004.** 27, 2049-2051.
20. Kevadiya, B. D.; Joshi, G. B.; Patel, H. A.; Ingole, P. G.; Mody, H. M.; and Bajaj, H. C. *J Biomater Appl.* **2010.** 25, 161-177.
21. Zheng J. P.; Luan, L.; Wang, X. Y.; Xi, L. F.; and Yao, K. D. *Appl Clay Sci.* **2007.** 36, 297-301.
22. Fejer, I.; Kata, M.; Eros, I.; Berkesi, O.; and Dekani, O. *Colloid Polym Sci.* **2001.** 279, 1177-1182.
23. Joshi, G. V.; Kevadiya, B. D.; Patel, H. A.; Bajaj, H. C.; and Jasra, R. V. *Int J Pharm.* **2009.** 374, 53-57.
24. Dong, Y.; and Feng, S. S. *Biomaterials.* **2005.** 26, 6068-6076.
25. Maisanaba, S.; Gutierrez-Praena, D.; Pichardo, S.; Moreno, F. J.; Jorda, M.; Camean, A. M.; Aucejo, S.; and Jos, Angeles. *J Appl Toxicol.* **2013.** 34, 714-725.
26. Phillips, T. D.; Afriyie-Gyawu, E.; Williams, J.; Huebner, H.; Ankrah, N. A.; Ofori-Adjei, D.; Jolly, P.; Johnson, N.; Taylor, J.; Marroquin-Cardona, A.; Xu, L.; Tang, L.; Wang, J. S. *Food Addit Contam A Chem Anal Control Expo Risk Assess.* **2008.** 25, 134-145.
27. Robinson, A.; Johnson, N. M.; Strey, A.; Taylor, J. F.; Marroquin-Cardona, A.; Mitchell, N. J.; Afriyie-Gyawu, E.; Ankrah, N. A.; Williams, J. H.; Wang, J. S.; Jolly, P. E.; Nachman, R. J.; Phillips, T. D. *Food Addit Contam A Chem Anal Control Expo Risk Assess.* **2012.** 29, 809-818.
28. Wiles, M.; Huebner, H.; Afriyie-Gyawu E; Taylor, R.; Bratton, G.; Phillips, T. J. *Toxicol Environ Health.* **2004.** 67, 863-874.
29. Zhang, K.; Xu, Z. P.; Lu, J.; Tang, Z. Y.; Zhao, H. J.; Good, D. A.; and Wei, M. Q. *Int J Mol Sci.* **2014.** 15, 7409-7428.
30. Xu, Z. P.; Walker, T. L.; Liu, K.; Cooper, H. M.; Lu, G. M.; and Bartlett, P. F. *Int J Nanomedicine.* **2007.** 2, 163-174.
31. Ladewig, K.; Niebert, M.; Xu, Z. P.; Gray, P. P.; and Lu, G. Q. *Appl Clay Sci.* **2010.** 48, 280-289.
32. Ladewig, K.; Xu, Z. P.; Lu, G. Q. *Expert Opin Drug Deliv.* **2009.** 6, 907-922.
33. Arruda, C. C.; Cardoso; P. H. L.; Dias, I. M. M.; and Salomao, R. *Interceram Refractories.* **2013,** 62, 187-191.

34. Nakayama, H.; Hatakeyama, A.; and Tshako, M. *Int J Pharm.* **2010.** 393, 105-112.
35. Kim, T.H.; Lee, G.J.; Kang, J.H.; Kim, H.J.; Kim, T.I.; Oh, J.M. *Biomed Res Int.* **2014.** 193401.
36. Barahuie, F.; Hussein, M. Z.; Gani, S. A.; Fakarazi, S.; and Zainal, Z. *Int J Nanomedicine.* **2014.** 9, 3137-3149.
37. Ma, R.; Wang, Z.; Yan, L.; Chen, X.; Zhu, G. *J Mater Chem.* **2014.** B2, 4868–4875.
38. Li, S.; Li, J.; Wang, C.J.; Wang, Q.; Cader, M.Z.; Lu, J.; Evans, D.G.; Duan, X.; O'Hare, D. *J Mater Chem.* **2013b.** B1, 61–68.
39. Wong, Y.; Markham, K.; Xu, Z. P.; Chen, M.; Lu, G. Q.; Bartlett, P. F.; and Cooper, H. M. *Biomaterials.* **2010.** 31, 8770-8779.
40. Ladewig, K.; Niebert, M.; Xu, Z. P.; Gray, P. P.; and Lu, G. Q. *Biomaterials.* **2010.** 31, 1821-1829.
41. Li, L., Gu, W.; Chen, J.; Chen, W.; and Xu; Z. P. *Biomaterials.* **2010.** 35, 3331-3339.
42. Mollaie, H. R.; Monavari, S. H. R.; Arabzadeh, S. A. M.; Shamsi-Shahrabadi, M.; Fazlalipour, M.; and Afshar, R. M. *Asian Pac J Cancer Prev.* **2013.** 14, 7045-7056.
43. Uchino, K.; Ochiya, T.; and Takeshita, F. *Jpn J Clin Oncol.* **2013.** 43, 596-607.
44. Lee, J. Yoon, T.; and Cho, Y. *Biomed Res Int.* **2013.**
45. Mansoori, B.; Shotorbani, S. S.; and Baradaran, B. *Adv Pharm Bull.* 4, 313-321.
46. Bender, E. (2014) The second coming of RNAi. *The Scientist.* <<http://www.the-scientist.com/?articles.view/articleNo/40871/title/The-Second-Coming-of-RNAi>>
47. Sanderson, B. A.; Araki, N.; Lilley, J. L.; Guerrero, G.; and Lewis, L. K. *Anal Biochem.* **2014.** 454, 44-52.
48. Tataurov, A. V.; You, Y.; and Owczarzy, R. *Biophysical Chemistry.* **2008.** 133, 66-70.
49. Moore, P.B. *The RNA World.* **1999.** 2, 381-400.
50. Biro, J. C. *Theor Biol Mel Model.* **2012.** 9, 10.
51. Mills, S. J.; Christy, A. G.; Genin, J. R.; Kameda, T.; and Colombo, F. *Mineral Mag.* **2012.** 76 (5), 1289 – 1336.

52. Lipman, R. S. A.; and Hou, Y. M. *Proc. Natl Acad Sci.* **1998.** 95, 13495-13500.
53. Wang, J.; Kalinichev, A. G.; Kirkpatrick, J.; Hou, X. *Chem Mater.* **2001.** 13, 145-150.
54. Ishihara, S.; Sahoo, P.; Deguchi, K.; Ohki, S.; Tansho, M.; Shimizu, T.; Labuta, J.; Hill, J. P.; Labuta, J.; Hill, J. P.; Ariga, K.; Watanabe, K.; Yamauchi, Y.; Suehara, S.; and Iyi, N. *JACS.* **2013.** 135: 18040-18043.
55. Franchi, M.; Ferris, J. P.; and Gallori, E. *Orig Life Evol Biosph.* **2002.** 33, 1-16.
56. Hashizume, H.; Van der Gaast, S.; and Theng, B.; K., G. *Evol Biol: Exobiology and Evolutionary Mechanisms.* **2013,** 61-78.
57. Ferris, J. P. *Elements.* **2005.** 1, 145-149.
58. Essington, M. E. *Soil and water chemistry: An integrative approach.* 2, 394.
59. Na, P., Zhang, F., Li, Y. *Acta Physico-Chimica Sinica.* **2006.** 22(9), 1137-1142.
60. Misra, V.K.; and Draper, D.E. *Biopolymers.* **1999.** 48, 113-135.
61. Nguyen, T. H.; and Chen, K. L. *Environ. Sci Technol.* **2007.** 41, 5370 – 5375.
62. Xu, W.; Johnston, C. T.; Parker, P.; and Agnew, S. F. *Clays Clay Miner.* **2000.** 48, 120-131.
63. Saeki, K.; Kunito, T.; and Sakai, M. *Microbes Environ.* **2011.** 26, 88-91.
64. Keren, R.; and O'Connor, G. A. *Clays Clay Miner.* **1982.** 30, 341-346.
65. Liu, Q.; Li, X.; and Sommer, S. S. *Anal Biochem.* **1999.** 270, 112-122.